

Lessons from (triggered) tremor

Joan Gomberg¹

Received 29 September 2009; revised 12 May 2010; accepted 2 June 2010; published 8 October 2010.

[1] I test a “clock-advance” model that implies triggered tremor is ambient tremor that occurs at a sped-up rate as a result of loading from passing seismic waves. This proposed model predicts that triggering probability is proportional to the product of the ambient tremor rate and a function describing the efficacy of the triggering wave to initiate a tremor event. Using data mostly from Cascadia, I have compared qualitatively a suite of teleseismic waves that did and did not trigger tremor with ambient tremor rates. Many of the observations are consistent with the model if the efficacy of the triggering wave depends on wave amplitude. One triggered tremor observation clearly violates the clock-advance model. The model prediction that larger triggering waves result in larger triggered tremor signals also appears inconsistent with the measurements. I conclude that the tremor source process is a more complex system than that described by the clock-advance model predictions tested. Results of this and previous studies also demonstrate that (1) conditions suitable for tremor generation exist in many tectonic environments, but, within each, only occur at particular spots whose locations change with time; (2) any fluid flow must be restricted to less than a meter; (3) the degree to which delayed failure and secondary triggering occurs is likely insignificant; and 4) both shear and dilatational deformations may trigger tremor. Triggered and ambient tremor rates correlate more strongly with stress than stressing rate, suggesting tremor sources result from time-dependent weakening processes rather than simple Coulomb failure.

Citation: Gomberg, J. (2010), Lessons from (triggered) tremor, *J. Geophys. Res.*, 115, B10302, doi:10.1029/2009JB007011.

1. Introduction

[2] I test the hypothesis that triggered tremor is likely nothing more than “clock-advanced” ambient tremor or, equivalently, ambient tremor that occurs at a sped-up rate as a result of the additional loading associated with passing seismic waves. The “clock-advance” model was developed and has been applied to explain triggered earthquakes [e.g., Dieterich, 1994; Gomberg *et al.*, 2000, 2005; Beeler *et al.*, 2003, 2007; Hardebeck, 2004; Kaneko and Lapusta, 2008]. In its most general form, the clock-advance model implies that a perturbing deformation change will alter the rate (probability) of failure, with the new rate depending on both the deformation change and the ambient (unperturbed) rate. Thus, a greater ambient rate corresponds to a greater likelihood of triggering.

[3] I test this hypothesis that a clock-advance model explains tremor triggered by passing seismic waves using observations and inferences described herein and others from previously published studies. If a clock-advance model is appropriate, then the observation of triggered tremor potentially provides a proxy for elevated rates of tremor and slow slip. Mounting evidence indicates that tremor sources

are likely causally related to slow slip inferred to occur on the interface between subducting and overlying plates [Rogers and Dragert, 2003; Obara *et al.*, 2004; Obara, 2009; Voison *et al.*, 2008; Aguiar *et al.*, 2009; Wech *et al.*, 2009]. Triggered tremor as a proxy for slow slip could be extremely useful because triggered tremor observation potentially only requires data from triggered recording seismic stations (i.e., that turn on only when large amplitude waves arrive). These operate in many more places globally than the continuously recording seismic and geodetic stations needed to observe ambient tremor and slow slip, respectively. In addition to their potential as a proxy for ambient tremor and slow slip, triggered tremor observations also provide constraints on the probable physical mechanisms that underlie the tremor source.

[4] “Ambient” tremor in the context of this study refers to tremor energy that waxes and wanes, possibly in concert with the rate or amplitude of slow slip [Aguiar *et al.*, 2009; Maeda and Obara, 2009; Payero *et al.*, 2008; Peterson *et al.*, 2007; and references therein]. Periods of geodetically measurable slow slip consistent with relaxation of plate convergence and nearly continuous tremor activity are commonly referred to as “episodic tremor and slip” (ETS) events, and recent observations show that tremor likely occurs at some rate all the time [Wech and Creager, 2008].

[5] The essence of “triggered” tremor observations is captured in Figure 1, taken from Rubinstein *et al.* [2007]. This figure shows the recorded surface displacement field

¹U.S. Geological Survey, Department of Earth and Space Sciences, University of Washington, Seattle, Washington, USA.

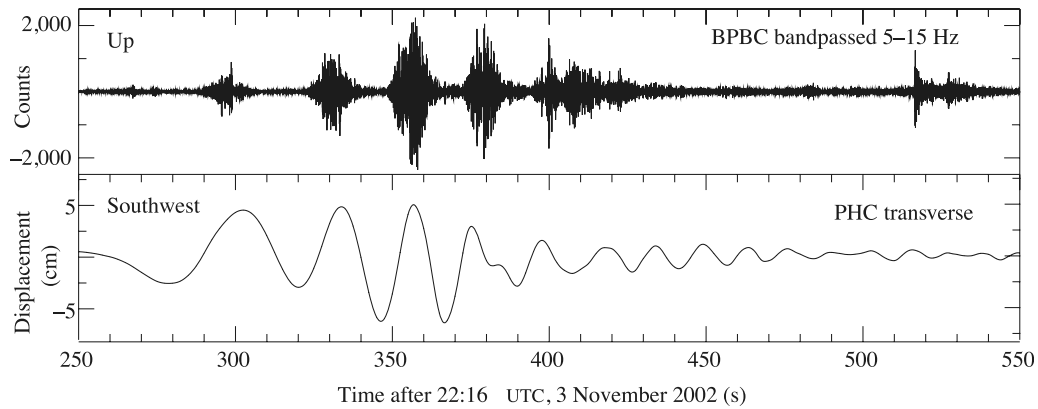


Figure 1. Example of triggered tremor, taken from Figure 3 of *Rubinstein et al.* [2007]. This figure shows tremor triggered by the Love waves radiated from the 2002 M7.9 Denali, Alaska. Top waveform shows tremor at station BPBC, shifted by 5.14 s to reflect the travel time of S waves from the tremor source to BPBC. Bottom waveform is the instrument-corrected, transverse displacement seismogram from station PHC. It has been shifted by 5.14 s to account from the travel time between the tremor source and station.

associated with the surface waves radiated from the 2002 Denali earthquake as they passed across Vancouver Island, British Columbia in northern Cascadia (Figure 2). These recordings provide a temporally high-resolution proxy for the wave-generated stresses acting on the interface between the subducting Juan de Fuca and overlying North American plates. Also shown in Figure 1 are high-frequency waveforms recorded at a nearby site that contain tremor signals that are synchronous with the much lower-frequency, larger amplitude Denali earthquake-generated Love waves. The relative phasing of the tremor bursts and Love wave peaks is consistent with tremor sources being triggered by wave-generated stresses that enhance failure otherwise promoted by plate convergence [*Rubinstein et al.*, 2007].

[6] A benefit of studying triggered tremor is that, in contrast to ambient tremor driven by slow slip, the temporal resolution of the triggering deformation can be estimated with temporal precision of the order of seconds. In contrast, the precise temporal relationship between ambient tremor and slow slip, such as which comes first, remains uncertain due to the emergent nature of the signals that constrain them. At best, in a few examples, *McCausland et al.* [2008] have shown that the simultaneity of the onsets of tremor and slow slip detected on borehole strainmeters can be resolved within about 30 minutes. For triggered tremor, the delays between triggering deformations and triggered tremor are resolvable within seconds. Although one cannot measure directly the stresses at the likely depths of the tremor sources, the long wavelengths of the triggering waves permit useful estimates of these stresses from surface recordings of the broadband displacement or velocity wave field and correlation of individual tremor bursts with particular wave-enhanced stress components [*Rubinstein et al.*, 2007, 2009; *Peng and Chao*, 2008; *Peng et al.*, 2009].

2. Framework Triggered Tremor Observations and Inferences

[7] Observations of triggered tremor from this and previous studies [*Rubinstein et al.*, 2007, 2009; *Peng and*

Chao, 2008; *Miyazawa and Mori*, 2006; *Miyazawa et al.*, 2008; *Gomberg et al.*, 2008; *Peng et al.*, 2009] reveal key features of tremor source processes. I summarize these observations and inferences drawn from them because they provide constraints on the processes underlying tremor generation and a framework for the hypothesis that triggered tremor is clock-advance tremor.

2.1. Triggered and Ambient Tremor

[8] As in other studies, I assume that triggered and ambient tremor reflect the same failure process [*Peng et al.*, 2008, 2009; *Rubinstein et al.*, 2007, 2009, 2010]. *Rubinstein et al.* [2007] showed that the amplitude spectrum of the triggered tremor has the same frequency dependence as ambient tremor. Like ambient tremor, triggered tremor also seems to be amplitude-limited [*Rubinstein et al.*, 2007; *Gomberg et al.*, 2008; *Miyazawa and Mori*, 2005, 2006; *Miyazawa and Brodsky*, 2008; *Peng et al.*, 2008].

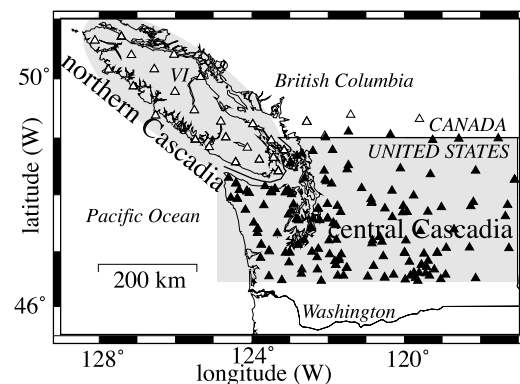


Figure 2. Map of the study region. Areas covered by the two tremor catalogs used are shown in grey. VI denotes Vancouver Island and triangles show the locations of seismic stations belonging to the CNSN (white) and PNSN (black), although data from stations near the border are shared.

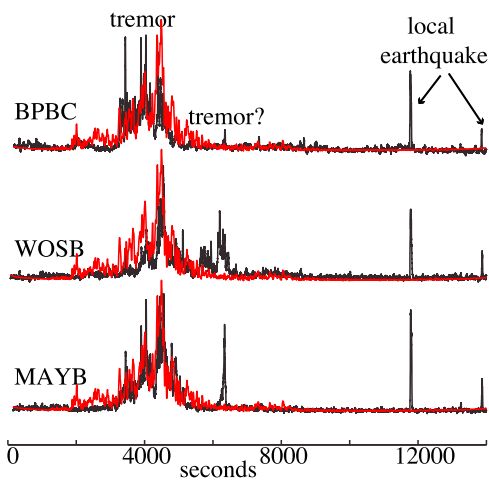


Figure 3. Temporal correlation between triggering waves and triggered tremor. Envelopes of broadband seismograms at station PHC (red) overlaid on vertical component seismograms at the nearby stations (labeled) that have been filtered in the passband 5–13 Hz to enhance the tremor signal, all from Vancouver Island during a 4 h window containing the arrival of waves from the 2004 M9.1 Sumatra earthquake. The envelopes have been smoothed with a 20 s moving-average filter and the PHC envelope is the square root of the sum of the squared amplitudes of all three components. I interpret the signals above the background noise level to be tremor in the high-frequency data and triggering surface waves from the Sumatra earthquake in the broadband data. A burst of tremor also appears delayed from the causative waves.

2.2. Widely Dispersed but Localized and Non-Stationary Triggering Conditions

[9] The growing numbers of tremor studies show that triggering tremor does not seem to require conditions unique to specific tectonic environments (e.g., hydration reactions associated with subduction), as triggered tremor has been observed in the subduction zones of Cascadia [Rubinstein *et al.*, 2007, 2009] and Japan [Miyazawa and Mori, 2005, 2006; Miyazawa and Brodsky, 2008; Miyazawa *et al.*, 2008], the collisional zone of Taiwan [Peng and Chao, 2009], and the transform boundary along the San Andreas fault in California [Gomberg *et al.*, 2008; Peng *et al.*, 2008, 2009].

[10] While observed in numerous regions, the conditions required for triggering tremor also appear to be highly localized and nonstationary within a given region. In both Cascadia [Rubinstein *et al.*, 2009] and along the San Andreas fault [Peng *et al.*, 2009] tremor has been triggered numerous times by waves from different earthquakes, and each time the tremor signals are explainable as radiating from a single or just a few point sources. In most cases, within each region no obvious differences were apparent in the waves arriving from different earthquakes, yet the tremor they triggered originated from different source locations. All of these observations suggest that the conditions necessary for triggering tremor exist in many places, but are only sufficient in very specific locales. Moreover, the locations of where these conditions exist may change temporally.

2.3. Triggering Deformation Mode

[11] In some cases, a strong correlation between triggering and triggered wave energy is apparent for Rayleigh waves [Miyazawa and Mori, 2005, 2006; Miyazawa and Brodsky, 2008; Miyazawa *et al.*, 2008], in others for Love waves [Rubinstein *et al.*, 2007; Peng *et al.*, 2008], and in others a correlation with either appears plausible [Rubinstein *et al.*, 2009; Peng *et al.*, 2009]. When resolved onto likely failure planes, the correlation between Rayleigh and/or Love wave peak amplitudes and triggered tremor bursts has been used to infer that dilatational or shear deformations, respectively, are the causative triggers. One interpretation that accommodates all this evidence is that tremor triggering involves a failure mechanism that depends on a Coulomb-type stress, which is composed of shear and normal stresses and pore pressures [Hill, 2010].

2.4. Nearly Immediate Failure Response, Secondary Triggering

[12] The observation of delayed triggering in earthquake failure has provided significant constraint on earthquake frictional failure [Dieterich, 1994; Gomberg *et al.*, 2000] and stress transfer models (e.g., of secondary aftershocks triggered by preceding aftershocks [Felzer *et al.*, 2003; Helmstetter *et al.*, 2005; Marsan and Lengline, 2008]). Thus, whether triggered tremor occurs with some delay, as noted in Section 3, should similarly constrain models explaining tremor. In most observations of triggered tremor, including those in this study, failure has little delay after the application of the load. When plausibly correlated with particular wave types and phases, this delay appears to be less than a few seconds. Figure 3 shows one of the five examples of triggered tremor examined in this study, from northern Cascadia for the waves radiated by the M9.0 2004 Sumatra earthquake. As in the other three cases there [Rubinstein *et al.*, 2009], triggered tremor was nearly synchronous with the triggering deformations.

[13] If fluid diffusion is involved in tremor generation, delays of a few seconds or less limit the distances fluids can travel to less than meter (and likely less). This distance limit may be estimated from inferred values of permeability and Darcy's Law. The latter predicts a diffusion length equal to $2\sqrt{cT_{dif}}$ in which c is hydraulic diffusivity and T_{dif} is a time interval. The diffusivity equals the ratio of the permeability over the product of the effective compressibility and fluid viscosity, and for these I assume values of $5 \times 10^{-11} \text{ Pa}^{-1}$ and 10^{-4} Pa s , respectively [Rice, 2006; Segall and Rice, 2006]. Permeabilities may reach $\sim 10^{-15} \text{ m}^2$ in the rocks surrounding fault zones, but within fault cores are approximately 10^{-19} to 10^{-20} [Segall and Rice, 2006]. Even lower permeabilities of 5×10^{-25} to $5 \times 10^{-22} \text{ m}^2$ have been inferred in the region of slow slip and tremor in Cascadia [Audet *et al.*, 2009]. These correspond to a range of hydraulic diffusivities of $\sim 0.2 \text{ m}^2/\text{s}$, $\sim 10^{-5} \text{ m}^2/\text{s}$, to $\sim 10^{-9} \text{ m}^2/\text{s}$. Thus, for a time interval of $T_{dif} \sim 2 \text{ s}$, the diffusion lengths equal $\sim 1 \text{ m}$ for the most permeable rocks, $\sim 1 \text{ cm}$ for rocks within the fault core, and fractions of a mm for the very lowest permeabilities inferred by Audet *et al.* [2009].

[14] Figure 3 also shows a burst of tremor arriving hundreds of seconds after the triggering broadband wave-train amplitude has returned to its pre-event level. This is

evidence of delayed or secondary triggering. The likelihood that this later pulse is ambient tremor is very low because the triggering waves arrived after a period of weeks in which no ambient tremor was detected [Rubinstein *et al.*, 2009]. The very small amplitude of most tremor, typically a factor of 2 to less than 10 above the background noise level, makes it difficult to determine whether tremor arriving after the primary triggering waves have passed is common or represents delayed or secondary triggering.

3. Is Triggered Tremor Clock-advance Ambient Tremor?

[15] For reasons summarized herein, I hypothesize that triggered tremor may be explained by the clock-advance model developed to explain triggered earthquakes [Dieterich, 1994; Gomberg *et al.*, 2000; Kaneko and Lapusta, 2008]. I test this hypothesis using newly available catalogs of ambient tremor from Cascadia [Kao and Shan, 2004; Wech and Creager, 2008; Wech *et al.*, 2009]. I treat northern Cascadia (Vancouver Island) and central Cascadia separately because the data sources differ for each region (Figure 2). The two regions are monitored by different, but overlapping seismic networks, namely the Canadian National Seismic Network (CNSN) operated by the Canadian Geological Survey in northern Cascadia and the Pacific Northwest Seismic Network (PNSN) operated by the University of Washington. Data from each network have been used independently to derive the two tremor catalogs described below. Triggered tremor has already been studied using northern Cascadia data [Rubinstein *et al.*, 2009], so I focus much of this work on a similar examination of triggered tremor using central Cascadia data. In both regions I also examine the correlation of triggered tremor with ambient tremor activity. Peng *et al.* [2009] have conducted a similar study of the Parkfield, California region, and I comment on their relevant results in the Discussion.

[16] Figure 4 illustrates the clock-advance model schematically. A volume of crust contains an ensemble or population of fault patches, each at different stages in their failure cycles. Under ambient conditions, the patches fail at rates governed by tectonic motions and by slow slip on a larger fault plane. The tremor patches need not lie on the slowly slipping plane (Figure 4a). Note that tremor may occur either as a direct consequence of the slip on the larger fault, or indirectly by some other process operating in concert with the slow slip. Because failure rate is proportional to a probability density describing the likelihood of failure [Beeler *et al.*, 2003, 2007], the terms “rate” and “probability” may be used interchangeably. In the clock-advance model, a perturbing deformation change will alter the rate, or probability of failure, with the new rate depending on both the deformation change and the ambient (unperturbed) rate. Thus, a greater ambient failure rate corresponds to a greater likelihood of triggering. In this application of the model, the ambient failure rate is approximately constant in the absence of slow slip (Figure 4b) and is time-varying during times of slow slip (Figure 4c). Passing seismic waves impart a transient perturbation to the tremor patches, advancing their failure times and increasing the failure rate. The change in the failure time of each patch is referred to as the clock-advance, Δt . For some failure mechanisms, the

perturbed failure rate change may last for some duration (Figures 4e–f). One such class of failure mechanisms involves self-accelerating processes such as frictional sliding or critical crack growth.

[17] Although only the simplest, qualitative predictions of the clock-advance model are tested in this study, I present a very general mathematical statement of the clock-advance model because it provides some additional insights. More detailed discussions of the model can be found elsewhere, particularly its analytic or numerical implementation and quantitative applications [e.g., Dieterich, 1994; Gomberg *et al.*, 2000, 2005; Beeler *et al.*, 2003, 2007; Hardebeck, 2004; Kaneko and Lapusta, 2008]. In its most general form, the model states that instantaneous perturbed seismicity rate r is a product of the unperturbed rate r_0 and a function that describes how the perturbing stress alters the failure times of each fault in the affected fault population [Dieterich, 1994; Gomberg, 2000; Gomberg *et al.*, 2005], or

$$r(t) = r_0(t - \Delta t) \times \left[1 - \frac{d\Delta t}{dT}(t) \right]^{-1} \quad (1)$$

T is the duration of the failure cycle and t is the time interval from the onset of the perturbation to failure. Note that equation (1) represents the instantaneous rate, and both the unperturbed and perturbed rates may be temporally varying (see Appendix A and Dieterich, 1994; Gomberg *et al.*, 2000, 2005; Beeler *et al.*, 2003, 2007; Hardebeck, 2004).

[18] The second term in equation (1), $(1 - \frac{d\Delta t}{dT})^{-1}$, describes the processes that govern how a perturbing deformation change affects failure of an individual fault patch, and is independent of any characteristics of the population. In essence, it describes the efficacy of a perturbation to bring a single fault to failure. This function can be derived analytically for fault patches with rate-state stick-slip frictional behavior subjected to a static stress change. When the ambient rate is constant, equation (1) leads to the same rate change model in Dieterich [1994] but is derived somewhat differently (see Gomberg *et al.*, 2000). The complete underlying physics and a functional form of the derivative in equation (1) are unknown for dynamic deformation changes such as those due to seismic wave passage [Gomberg, 2000], but I assume that larger waves lead to larger rate increases (i.e., $\frac{d\Delta t}{dT}$ increases with increasing wave amplitude). While other wave characteristics are important as well, a dependence on amplitude has been verified for stick-slip behavior in model calculations [Gomberg *et al.*, 1998; Belardinelli *et al.*, 2003; Voison *et al.*, 2002, 2004], in laboratory studies [Savage and Marone, 2007, 2008], and for real earthquakes [Felzer and Brodsky, 2006; Gomberg and Felzer, 2008].

[19] I suggest that the assumptions underlying the clock-advance model are better justified in the triggering of tremor than earthquakes, despite being developed for earthquakes and noting that the model certainly does not explain all cases of earthquake triggering. The clock-advance model assumes all sources have the same frictional properties and the sources do not interact with one another. When applied to aftershocks, the independence of sources implies that aftershocks themselves do not impart perturbing deformations to other aftershock faults. However, numerous studies have shown that aftershocks do contribute to the triggering of other

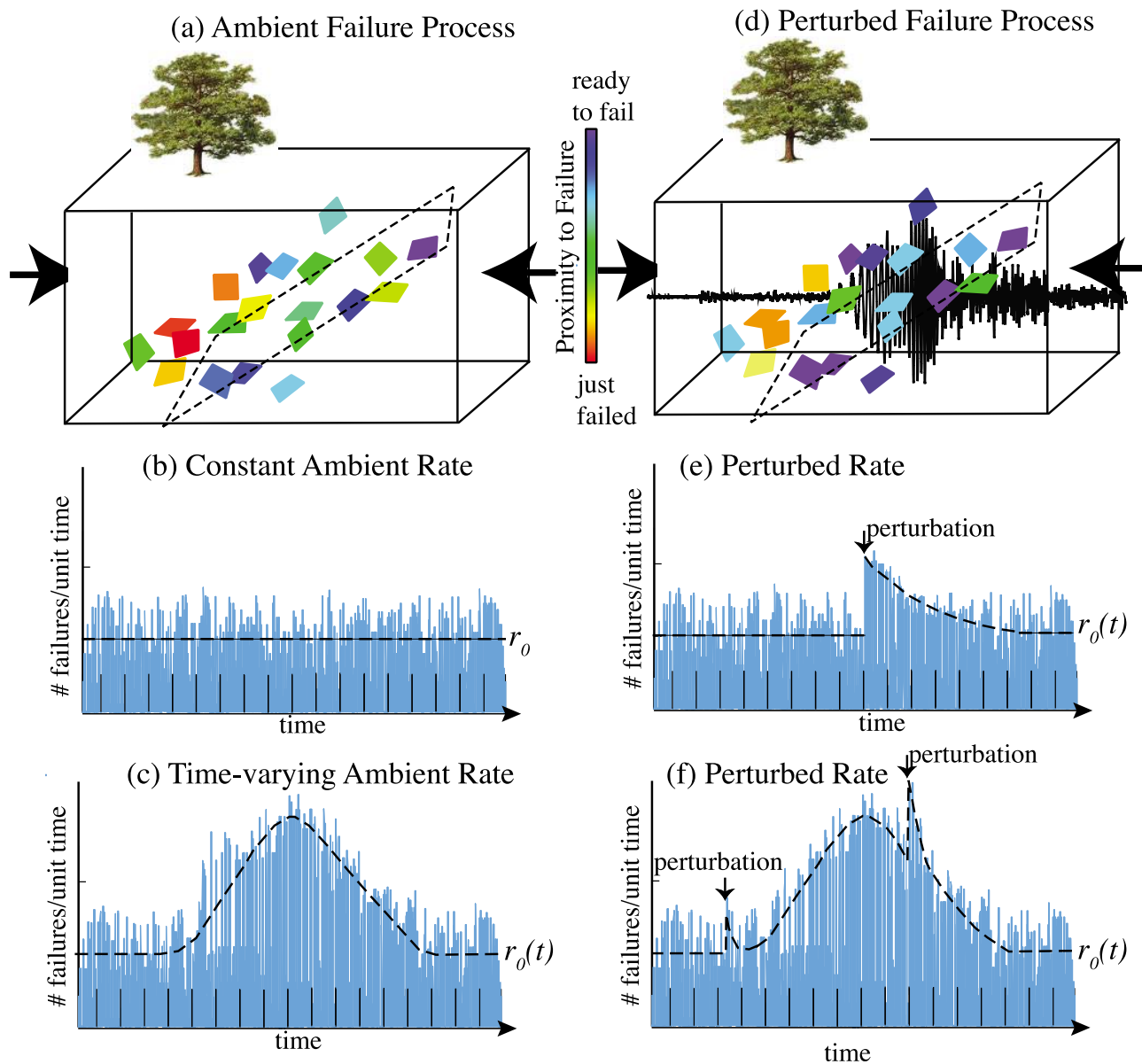


Figure 4. Cartoon of tremor and the clock-advance model. (a) Ensemble or population of fault patches (polygons), each at different stages in their failure cycles indicated by their color (e.g., red indicating patches that just failed, purple about to fail, etc.). Patches may be loaded by tectonic motions (arrows outside the box) and by slow slip on a larger fault plane (dashed rectangle), or secondarily by some other process related to these motions. Patches need not lie on the slipping plane. (b) Histograms of the number of failures per unit time in the absence of slow slip when loading is constant and failures occur at some constant average ambient rate r_0 (dashed line). (c) Same as Figure 4b but when slow slip leads to time-varying loading and a time-varying ambient failure rate, $r_0(t)$ (dashed curve). (d) Same as Figure 4a but now passing seismic waves impart an additional transient load to the tremor patches or indirectly through some intermediate process. (e) A rapid perturbation in the ambient loading advances the failure times of each patch resulting in a failure rate change that may last for some duration. Because r_0 is constant, the characteristics of the perturbed rate depend only on the perturbation and not when it's applied. (f) The perturbed rate depends on both a time-varying r_0 and the perturbation.

aftershocks [Felzer *et al.*, 2003; Marsan and Lengline, 2008], with the perturbing effect being larger for larger aftershocks. I envision a population of small tremor sources that have a much more limited range of sizes than earthquakes (Figures 4a,d), reasonable because unlike earthquakes, tremor amplitudes do not grow with the signal duration and

appear to have an upper limit [Ide *et al.*, 2007, 2008]. The variable and often extended duration of tremor signals thus reflects tremor sources radiating in succession, with occasional larger amplitudes resulting from the superposition of signals from multiple sources radiating simultaneously. The relative rarity of longer period radiation within tremor signals

[Ide *et al.*, 2007, 2008; La Rocca *et al.*, 2009] suggests that tremor sources do not fail coherently or interact with one another. Thus, this general lack of coherence and the smaller size distribution suggest that assumptions of independence of tremor sources may be more justified than for earthquake applications.

[20] Another reason the clock-advance model may be more appropriately applied to tremor than earthquakes is that the model fails to explain rate changes that have sustained durations or failure that is delayed significantly after a perturbing transient deformation (more than seconds to minutes). This is true for faults governed by conventional rock failure mechanisms or rate and state friction [Gomberg, 2001; Belardinelli *et al.*, 2003] and thus at least for these failure mechanisms, the model cannot explain triggering of most aftershocks by seismic waves. The reasons for this are explained in Appendix A. However, the inability to explain delayed failure is not so problematic for triggered tremor because, while some delayed triggered tremor cannot be ruled out, most tremor appears to trigger nearly immediately (see Section 2.3).

[21] Previous studies show that the likelihood of detecting triggered tremor clearly depends on the amplitude of the triggering waves such that, regardless of the ambient tremor rate, above and below some peak wave particle velocities (proportional to strain for a plane wave) triggering effectively does or does not occur, respectively [Rubinstein *et al.*, 2009; Peng and Chao, 2008; Peng *et al.*, 2009]. This is consistent with theoretical and laboratory experiments of the frictional response to transient loads [Richardson and Marone, 2008]. However, there is an intermediate amplitude range in which tremor is only sometimes triggered. For example, Rubinstein *et al.* [2009] and Peng *et al.* [2009] examine the relationship between triggered tremor and peak velocities of posited triggering teleseismic waves passing across Vancouver Island and Parkfield, California, respectively. Both studies show that while there appears to be wave particle velocities above and below which triggering does and does not occur, respectively, there is a range in between in which the probability of triggering depends on more than just the amplitude of the triggering deformation.

[22] The clock-advance model predicts that for waves in this intermediate range triggered, tremor is more likely when the ambient tremor rate is high or when the efficacy of the posited triggering waves is greater [equation (1)], which likely is the case when the waves have greater amplitude. By extension, an elevated ambient tremor rate could imply that the probability of triggering also depends on the rate of slow slip, and, thus, observations of tremor triggered by waves of this intermediate amplitude range would serve as indicators of ongoing slow slip. A connection between slow slip and tremor does not require that the tremor occur on the plate interface, only the two processes are somehow linked.

[23] If the clock-advance model hypothesis that the probability of triggering tremor correlates with the ambient tremor rate is true, triggered tremor is more likely to be observed when the ambient tremor rate is relatively high. I interpret tremor rates only qualitatively and in a relative sense. Tremor catalog heterogeneity is significantly more severe than for earthquake catalogs, spatially and temporally, and even in the definition of what is a tremor event. Each of the catalogs used defines an “event” differently, so

that a uniform measure and meaning of rate is not possible. None of the methods for detecting and cataloging tremor captures all tremor energy, so that the subset of the total tremor represented in each catalog likely varies. As many studies of more mature earthquake seismicity catalogs and derived rates have shown (e.g., see Marsan and Nalbant [2005]), even when events are similarly characterized, meaningful estimation of rates is challenging because estimates depend on properties like magnitude completion, data binning and smoothing, and choice of region, to name just a few. Future efforts within the community studying these processes might focus on some standardization of metrics of tremor size and duration; i.e., on what constitutes a tremor event.

3.1. Testing the Clock-advance Model Using Tremor Rates

3.1.1. Cascadia Tremor Catalogs and Rates

[24] Tremor rates using northern Cascadia data were calculated from a 1997–2007 tremor catalog derived using the “source scanning” method of Kao and Shan [2004]. This algorithm identifies and locates tremor sources by summing the squared amplitudes of ground velocities within a 1 s. window recorded at an array of stations with travel times computed for a sweep of origin times and hypocenters spanning the region. Summed amplitudes (“brightnesses”) exceeding some threshold illuminate a tremor source, with the duration of a source corresponding to the contiguous time interval the brightness remains above the threshold.

[25] Rate changes associated with triggering wave trains cannot be detected using the northern Cascadia tremor catalog because of the need to estimate rates averaged over time scales that are longer than the duration of the posited triggering wave trains. I estimate hourly-averaged tremor rates that are then smoothed over a 24 h. period. I do this so that there are enough measurements to obtain a meaningful rate estimate, noting that the catalog tremor rate rarely exceeds a few events/hour. I infer that this low catalog rate reflects conservative detection criteria because such low rates are reported even during ETS events when ambient tremor in some waveform data appears almost continuous. Additional corroboration of a high detection threshold comes from the fact that the catalog does not contain any of the triggered tremor events identified in Rubinstein *et al.* [2009]. In Figure 5 I plot the estimated tremor rates for the entire catalog duration and superpose the peak velocities of the earthquake waves studied in Rubinstein *et al.* [2009].

[26] The data used for the central Cascadia catalog come from the PNSN within the region of 46.5°–49.5°N and 117.0°–125.0°W (Figure 2). Details about the tremor catalog can be found in Wech and Creager [2008]. This catalog spans the entire time period of January 2007 through May 2008, which includes two ETS episodes, and the duration of two ETS episodes in July 2004 and September 2005. Automatically detected tremor events are catalogued based on the coherence of 50% overlapping signals lasting 5–minutes in the 1–8 Hz frequency band, across 20 stations of the PNSN and a few of the southern-most CNSN stations on Vancouver Island. Detection of tremor sources requires that the source of the energy be locatable using cross-correlation methods within a specified uncertainty, and spurious detections are eliminated by requiring that at least two sources occur within specified time and space windows. All tremor

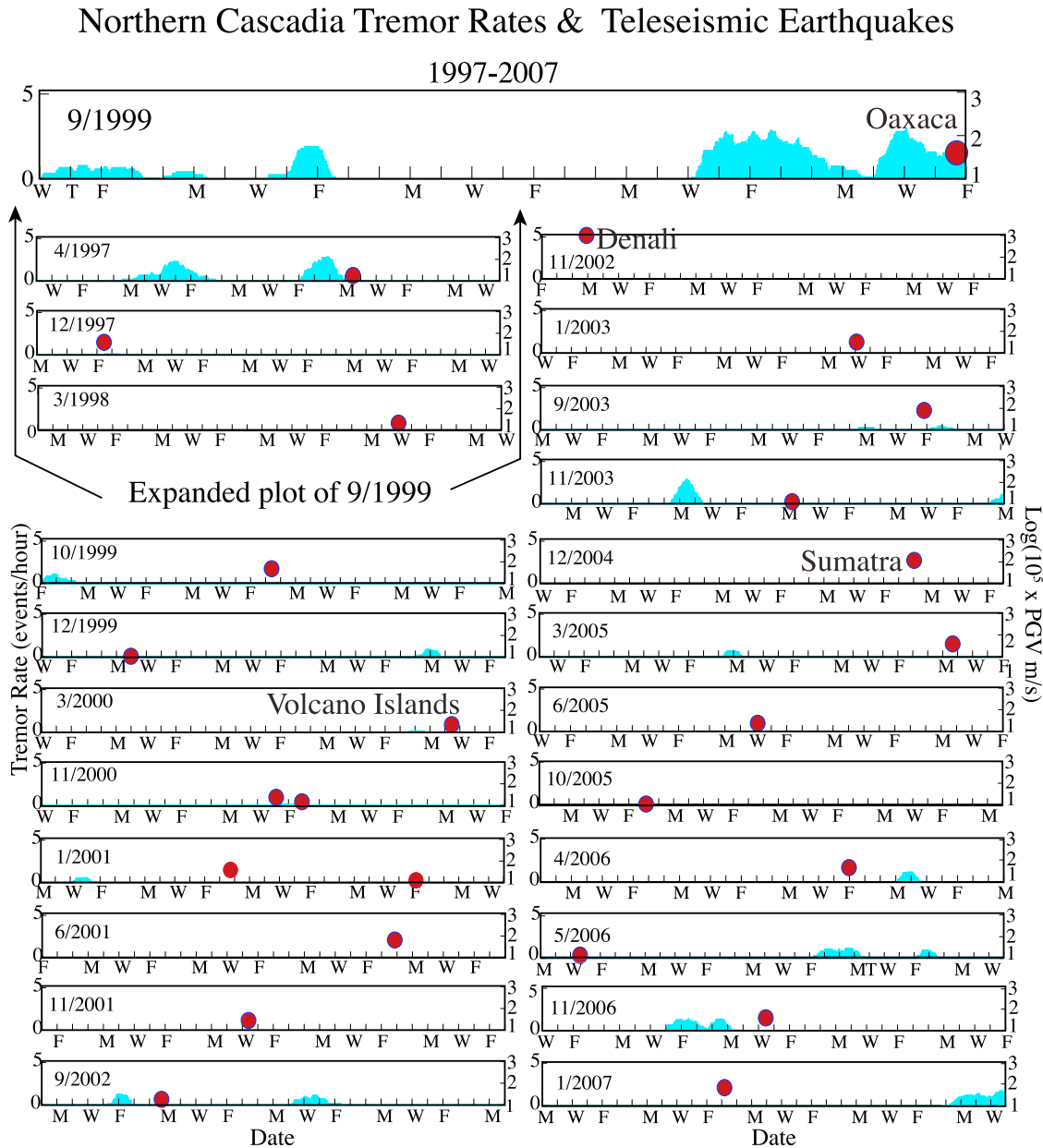


Figure 5. Northern Cascadia ambient tremor rates and posited triggering earthquakes. Hourly tremor rates (blue bars, left y-axes) computed from the Vancouver Island tremor catalog [Kao and Shan, 2004] and smoothed with a moving 24 h window, plotted only for months in which data from large teleseisms were examined (months labeled on the left). The origin times of the 26 earthquakes that radiated the largest waves that traversed Vancouver Island between 1997 and 2007 are plotted (red ovals) versus their corresponding peak velocities (right y-axes, from Rubenstein et al., 2009); those that triggered tremor are labeled. The one month containing both an ETS event and a large teleseism is shown at a larger scale at the top of the figure.

events thus have *a priori* fixed 5-minute event durations, and because of the overlapping, this limits the maximum rate to 18 events/hour. A tremor event duration also is comparable to the duration of the wave trains containing the posited triggered tremor signals. For reasons similar to those for the northern Cascade catalog, this fixed tremor duration precludes detection of significant rate changes associated with triggered activity. It should be noted that the PNSN receives some data from the more southerly stations of the

CNSN and that some tremor may be included in both the northern and central Cascadia catalogs.

[27] As for the northern Cascadia rates, I superpose on tremor rates estimated from the central Cascadia catalog the origin times of all $M > 7.0$ global earthquakes that occurred during this time period (Figure 6). I also include two $M \geq 6.6$ earthquakes in 2008, because they occurred about the time of an ETS event and were closer to Cascadia than the $M > 7.0$ earthquakes, and thus the waves arriving from them

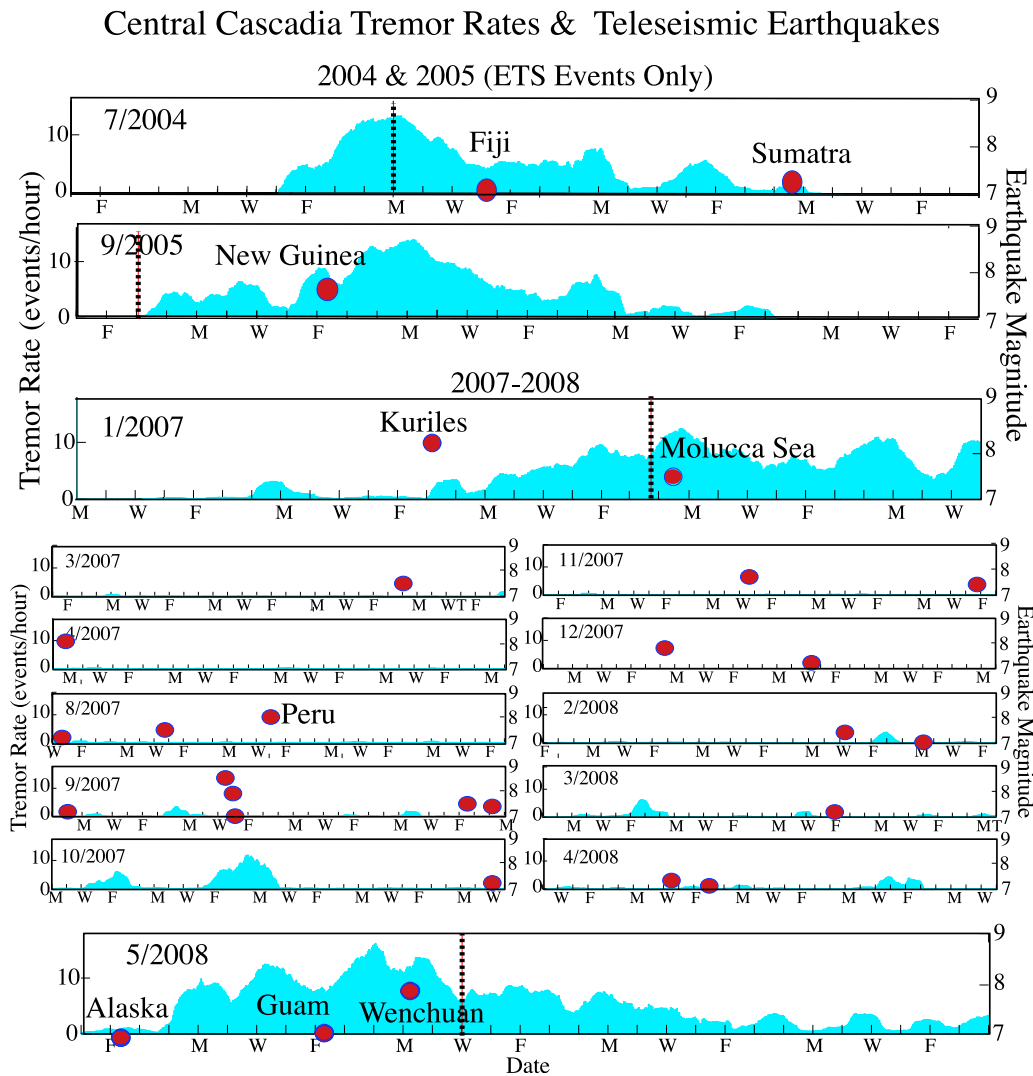


Figure 6. Central Cascadia ambient tremor rates and posited triggering earthquakes for all of January 2007 through May 2008 and the durations of the ETS events of 2004 and 2005. Each row is a plot of the smoothed hourly tremor rate (left axes). The origin times of all $M \geq 7.0$ earthquakes and two $M \geq 6.6$ just before and during the 2008 ETS event are plotted (red circles) versus their corresponding magnitudes (right y-axes). Labeled earthquakes are those for which I examined the waveform data closely. Only months in 2007–2008 containing earthquakes are plotted, and months containing ETS events are shown at a larger scale. Dashed vertical lines are the GPS-identified onsets of slow slip; note that these times are approximate as the slip migrates spatially. Recent strainmeter observations also show that the delayed onsets of GPS signals relative to the onsets of tremor rate increases and strainmeter signals suggest that the slow slip transient starts earlier but is not detectable with GPS [McCausland *et al.*, 2008].

could potentially have been larger. I plot magnitudes instead of peak velocities (as in Rubinstein *et al.* [2009]) because, while less informative, this eliminated the need to instrument correct all the data. However, to assess the dependence on triggering wave amplitude I examined waveforms radiated by the earthquakes labeled in Figure 6, and compared the relative peak velocities of all the posited triggering wave trains at the station SQM, which is located in the center of much of the ambient tremor located by the PNSN. I also compare qualitatively other features of the wave fields for each posited triggering event to those for the 2008 Wenchuan earthquake, which is the only case that clearly triggered tremor (see below). Because I consider long period

(~ 10 s period and longer), mostly teleseismic surface waves, the variation in amplitudes across the aperture of the PNSN should be less than that between earthquakes.

3.1.2. Triggered Tremor in Central Cascadia

[28] Triggered tremor has already been studied in northern Cascadia so in this study I focus on a comparable investigation for central Cascadia. I present the Wenchuan-triggered tremor observations first, because they serve as the reference-triggering signal in this region. Figure 7 shows a latitude-ordered record section of PNSN seismograms of the Wenchuan earthquake waves bandpass filtered between 2–10 Hz, with 3-component broadband seismograms from station SQM plotted below the record section to show the

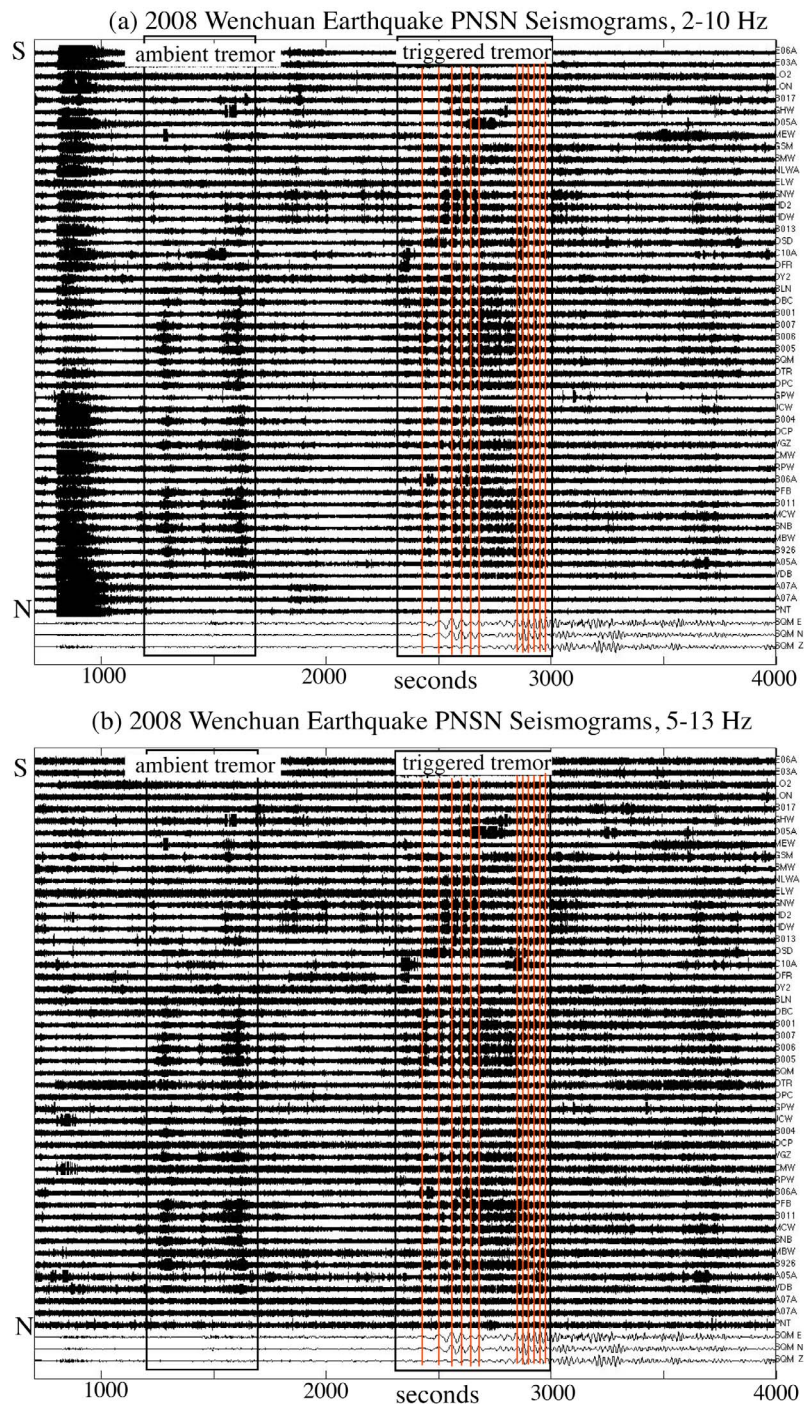


Figure 7. (a) Latitude-ordered record section of PNSN seismograms bandpass filtered between 2–10 Hz for the time interval in which Wenchuan earthquake waves traversed the region. Three-component broadband seismograms recorded at station SQM (bottom) show when posited triggering waves arrive. Boxes denote time intervals when ambient and triggered tremor signals arrive. (b) Same plot as Figure 7a except for a 5–13 passband. Red lines are drawn at the times of peaks in the Love and Rayleigh wave packets to make it easier to see the phase-locked nature between the waves and arrival of tremor energy.

synchronization of the tremor with the arrival and phasing of the surface waves. The Wenchuan earthquake occurred in the middle of the 2008 ETS event so that the tremor rate and by inference, the detection probability, were extremely high (Figure 6). Thus, coherent bursts of energy that arrive

between the P-wave and triggered tremor likely represent ambient tremor (Figure 7a). The large amplitude Wenchuan P-wave signal in Figure 7 also shows that significant 2–10 Hz body-wave energy from the triggering earthquake source is not attenuated. However, Wenchuan body-waves

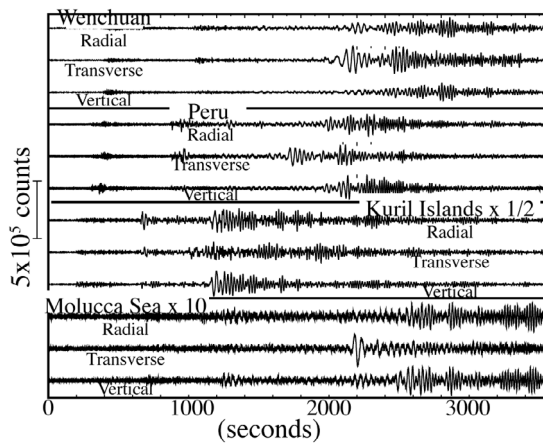


Figure 8. Broadband, 3-component waveforms of the 2 earthquakes that occurred at the onset and during the 2007 ETS event (the Kuril Island and Molucca Sea earthquakes, respectively), during a time of no detectable tremor (the Peru earthquake) and for reference, of the triggering 2008 Wenchuan earthquake (top). All data were recorded at station PNSN station SQM. A single amplitude scale is used, but the seismograms for the Kuril Island and Molucca Sea earthquakes have been scaled by the amounts listed.

and local tremor can be discriminated by looking in a higher frequency passband. The P-wave arrivals vanish when the same record section is made for a 5–13 Hz passband (Figure 7b), while the later coherent arrivals I interpret as tremor remain clear. Hereafter I present subsequent tremor

observations in the 2–10 Hz passband because the tremor is clearer, but minimize false detections in all tremor searches by examining both this and the 5–13 Hz passbands and a global catalog for arrivals from other earthquakes.

[29] I also examined data surrounding the arrival of the 2007 M8.0 Peru earthquake waves in order to test the null hypothesis that the probability of triggering has nothing to do with the ambient tremor rate and additionally that waves of comparable amplitude to those from the Wenchuan earthquake should trigger tremor, even during a time of no detectable ambient tremor. The 2007 M8.0 Peru earthquake waves are well suited to this hypothesis test (see Figures 6 and 8, and text below). As shown in Figure 9, they appear not to have triggered tremor.

[30] Waves from the two posited triggering earthquakes that occurred just prior to and during the 2007 ETS event, the M8.1 Kuril Islands and M7.5 Molucca Sea earthquakes (Table 1, Figure 8), failed to trigger tremor. Tremor is not apparent during the arrival of waves from the Kuril earthquake (Figure 10a). Tremor is visible during the period when waves from the Molucca Sea earthquake arrive (Figure 10b), but is likely ambient tremor because the catalog ambient rate is high, the tremor does not correlate with the arrival of any particular waves, nor is it modulated by the surface waves.

[31] No triggered tremor can be seen during the $M > 7$ teleseismic wave trains (Figure 11) that arrived during 2004, 2005, and 2008 ETS events (with the exception of the Wenchuan earthquake wave train). Small pulses coherent across multiple PNSN stations at the arrival time of likely depth phases from the July 2004 Sumatra earthquake in the

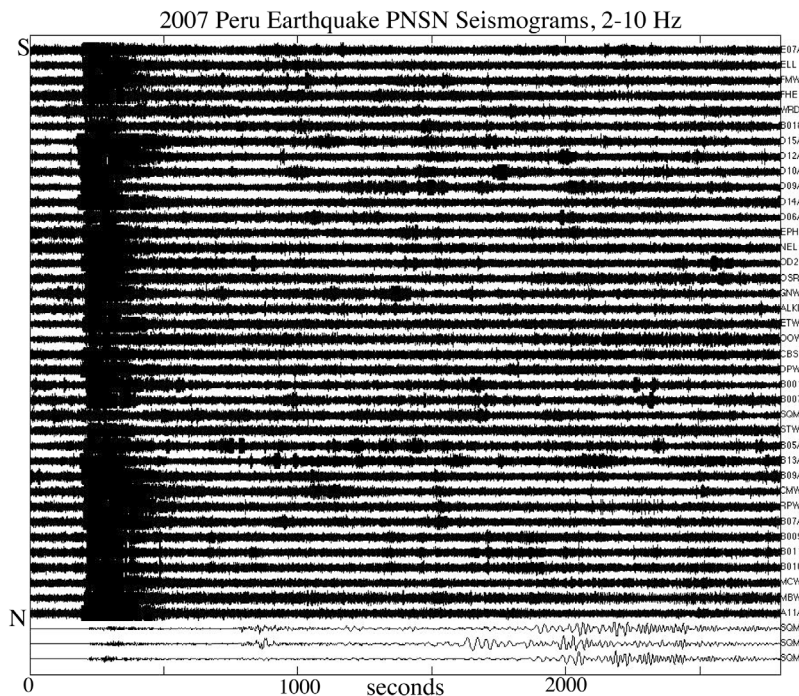


Figure 9. Latitude-ordered record section of PNSN seismograms bandpass filtered between 2–10 Hz for the time interval in which waves from the 2007 Peru earthquake (Table 1) traversed the region. Three-component broadband seismograms recorded at station SQM (bottom) show when posited triggering waves arrive.

Table 1. Earthquakes in Central Cascadia Data Set^a

Location/Label	Date	Time (UTC)	Latitude	Longitude	Depth (km)	M	Source-Receiver Distance (km)
Denali, Alaska	3 Nov 2002	2212:41	63.52	-147.53	5	7.9	2,383
Fiji	15 Jul 2004	0427:15	-17.66	-178.76	566	7.1	9,140
Sumatra	25 Jul 2004	1435:19	-2.43	103.98	582	7.3	13,252
Sumatra	26 Dec 2004	0058:53	3.316	95.854	30	9.1	13,158 ^b
New Guinea	9 Sep 2005	0726:44	-4.54	153.47	90	7.6	9,899
Kuril Islands	13 Jan 2007	0423:20	46.272	154.455	10	8.1	5,939
Molucca Sea	21 Jan 2007	1127:45	1.222	126.395	22	7.5	11,440
Peru	15 Aug 2007	2340:57	-13.354	-76.509	39	8.0	8,211
Alaska	2 Aug 2008	0133:36	51.935	-177.595	14	6.6	3,841
Guam	9 May 2008	2151:29	12.506	143.179	76	6.7	9,263
Wenchuan, China	12 May 2008	0628:01	30.986	103.364	19	7.9	10,105

^aEarthquake name or location, origin date and time, epicenter, depth, magnitude, and distance from the triggering earthquake to station SQM.

^bDistance is to station OPC instead of SQM.

2–10 Hz passband (Figure 12) are suggestive of tremor triggered by body waves, but these pulses and P-wave energy are diminished or absent in the 5–13 Hz passband (not shown) suggesting that both have a common origin at the source of the triggering earthquake. I performed the same types of examination for all other events in this group, but none showed any evidence of triggered tremor (Figure 12).

3.1.3. Triggered Tremor and Tremor Rates

[32] Table 2 presents a comparison of the amplitudes of the posited triggering waves, whether they triggered tremor, and the ambient tremor rate during the time interval in which they arrived (see also Figures 5 and 6). The amplitudes and rates are noted relative to those for a reference event, chosen because it is most consistent with the predictions of a clock-advance model. These reference wave trains clearly triggered tremor and arrived during an ETS event when the ambient rate was maximal. For the northern Cascadia data set, this is the 1999 Oaxaca earthquake, and for central Cascadia it is the 2008 Wenchuan earthquake. The 2010 M8.8 Chilean earthquake also provided a fortuitous set of observations that similarly corroborate the clock-advance model, having triggered tremor beneath Vancouver Island during a vigorous, unexpected episode of swarm activity and geodetic deformation in the same location as the triggered tremor. Because the Chilean earthquake occurred while this paper was being revised, I only note the most salient observations in the Conclusions section.

[33] The time periods relevant to testing the clock-advance model are determined by the intervals covered by the tremor catalogs. The two catalogs overlap only for the ETS events of 2004, 2005, and all of 2007. However, there is no overlap between the posited triggering wave trains I considered and the triggered tremor study of *Rubinstein et al.* [2009], which did not examine data during the 2004 or 2005 ETS events and only for one earthquake during January 2007 when an ETS event also occurred. While both *Rubinstein et al.* [2009] and I both selected data for time periods including $M > 7$ teleseismic earthquakes, apparently their criteria eliminated the five teleseisms I identified and examined. As shown in [Wech *et al.*, 2009], the distribution of tremor sources during the 2004 and later ETS events all began in central Cascadia or just at the boundary between the two regions and migrated mostly northward into southern Vancouver Island. In other words, for the 2004 and

later ETS events, the distributions of ambient tremor were centered in central Cascadia.

[34] Prior to 2004, testing of the clock-advance model relies on the triggered tremor observations of *Rubinstein et al.* [2009]. Their most compelling evidence for a clock-advance model is the triggering of tremor by the waves from the M7.5 1999 Oaxaca earthquake (Figure 5). As noted below, larger waves passed through, but the Oaxaca earthquake waves arrived in the middle of an ETS event and the source of the tremor it triggered locates within the distribution of ambient tremor sources. *Rubinstein et al.* [2009] also identified tremor triggered by smaller waves than those from the Oaxaca event, radiated by the M7.6 2000 Volcano Islands earthquake. This observation contradicts the predictions of the clock-advance model, because the waves arrived during a time devoid of catalogued ambient tremor. Several explanations are possible, although none are very satisfying. Perhaps this represents the chance, low probability occurrence of a single patch being very ripe for failure just when the waves from this earthquake passed through the region. Another possibility is that the triggering waves passed at a time when the noise levels were unusually low.

[35] For the pre-2004 period, it is also noteworthy that waves from the M8.3 2003 Tokachi-Oki earthquake had two and four times the amplitudes of those from the triggering Oaxaca and Volcano Island earthquakes, respectively, but the Tokachi-Oki earthquake waves failed to trigger tremor. These larger waves arrived when tremor rates were much lower than when the waves from the Oaxaca earthquake arrived (see Table 2), which is consistent with the clock-advance model prediction that the ambient tremor rate plays a key role in the probability of triggering. As noted above, triggering by the smaller Volcano Island earthquake waves suggests that triggering potential depends on neither the ambient rate nor the wave amplitude and is inconsistent with clock-advance model predictions.

[36] *Rubinstein et al.* [2009] did not look for triggered tremor during ETS events from 2004–2007, but they did look at intervals in this time period surrounding eight $M > 7.0$ teleseisms. No tremor was detected in the northern Cascadia catalog for seven of these, consistent with a clock-advance model. The exception was the wave train from the M9.1 2004 Sumatra earthquake, and *Rubinstein et al.* [2009] suggest that it and the triggering waves from the M7.9

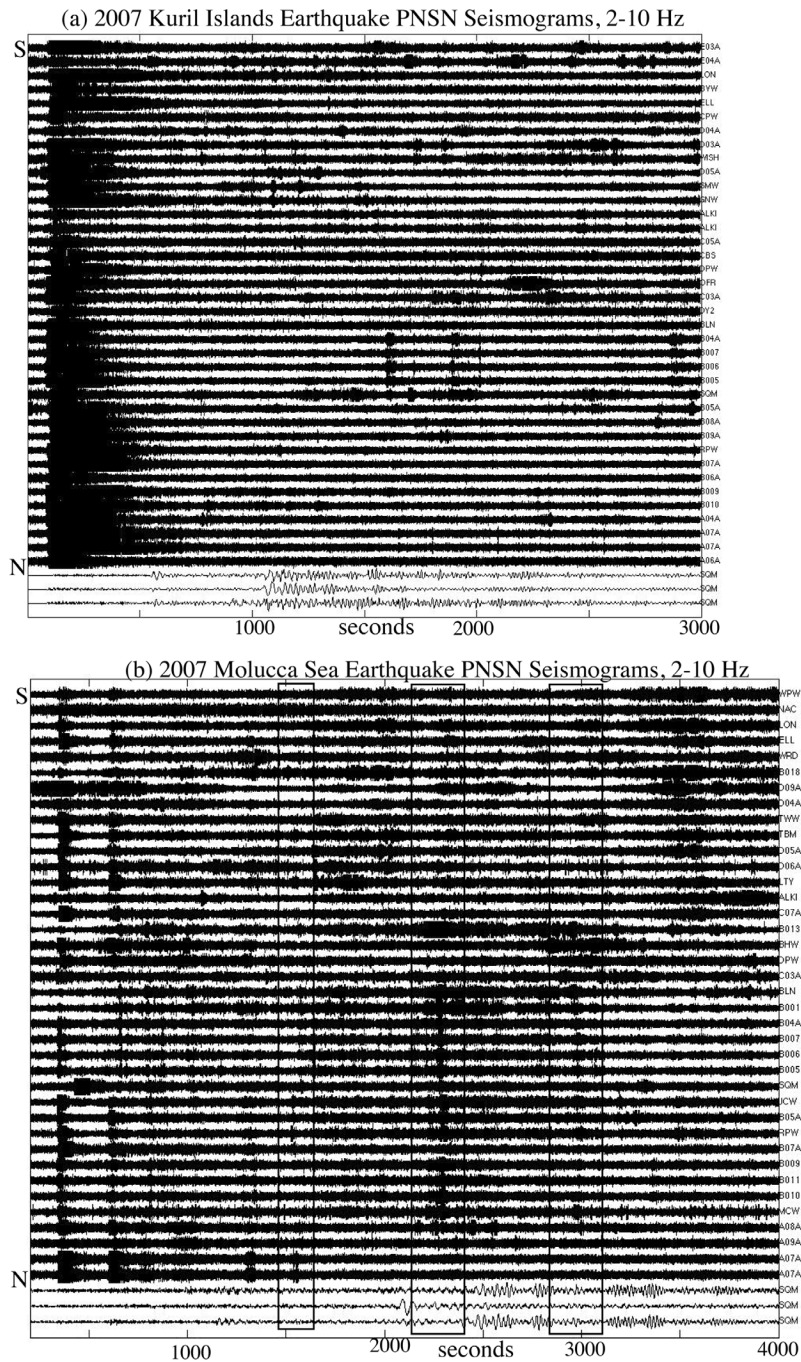


Figure 10. (a) Record-section of PNSN waveforms filtered between 2–10 Hz arranged by recording-station latitude during the arrival of waves from the 2007 M8.1 Kuril Islands earthquake. The only energy that is clearly coherent across multiple stations is from the P-wave of the Kuril Islands earthquake itself. This energy vanishes if the data are filtered in the 5–13 Hz passband. The bottom 3 traces show the posited-triggering, broadband, 3-component waveforms recorded at station SQM. (b) Same type of record section except the time window corresponds to the arrival of waves from the 2007 M7.5 Molucca Sea earthquake. I interpret tremor to be the coherent arrivals apparent both in the 2–10 Hz and 5–13 Hz passband, within the time windows denoted by the rectangles. Other coherent energy vanishes in the 5–13 Hz band and thus is interpreted as coming from the Molucca Sea earthquake source region, rather than from locally triggered tremor sources.

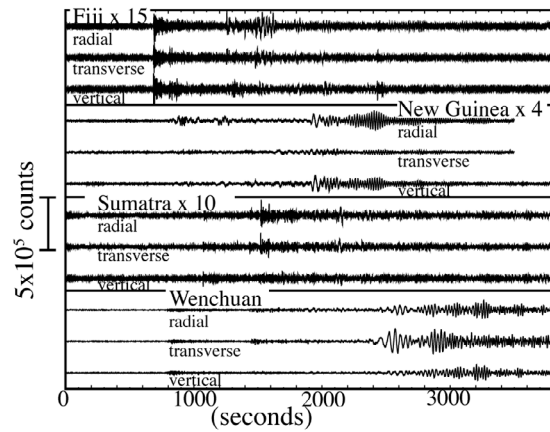


Figure 11. Broadband 3-component waveforms of the 3 earthquakes that occurred during the 2004 and 2005 ETS events (top 3 panels) and, for reference, of the triggering 2008 Wenchuan earthquake (bottom). All data were recorded at station PNSN station SQM. A single amplitude scale is used, but the seismograms for all but the Wenchuan earthquake have been scaled by the amount listed with the name of the earthquake.

2002 Denali, Alaska earthquake were so extraordinarily large that triggering was highly probable in some location regardless of the ambient tremor rate (Table 2). This is consistent with the predictions of some rate-state frictional model calculations [Belardinelli *et al.*, 2003; Richardson and Marone, 2008]. These two earthquakes did not appear to trigger tremor in central Cascadia, but the data from both regions suggest that the detection threshold was likely higher in central Cascadia as well (see Appendix B).

[37] Examination of the correlation between tremor rate and triggered tremor during the ETS events of 2004, 2005, 2007, and 2008 is possible only for the catalog from central Cascadia (Figure 6). I have also examined this correlation during the inter-ETS time periods using this catalog and my investigation of triggered tremor described in the previous section.

[38] Perhaps the most motivating observation for this study is of tremor triggered by the 2008 Wenchuan earthquake waves (Figure 7). In addition to passing through the region in the midst of an ETS episode like the triggering Oaxaca earthquake waves (Figure 6), this was the only clear case of triggered tremor in the central Cascadia data set, with the caveat that detection thresholds were likely higher in this part of Cascadia relative to Vancouver Island until sometime after 2004 (see Appendix B). Cross correlation analyses performed to estimate the source locations of the Wenchuan-triggered tremor indicate multiple sources, all within the same distribution of ambient tremor sources concentrated in central Cascadia at the time (A. Wech, personal communication). These analyses included data from the more southerly CNSN stations, and data from others in northern Cascadia were examined but revealed no evidence of sources outside the distribution of ambient ETS tremor.

[39] Comparable or larger waves to those from the Wenchuan earthquake passed through central Cascadia during times when ambient tremor was relatively quiescent and no triggered tremor was detected. In particular, waves

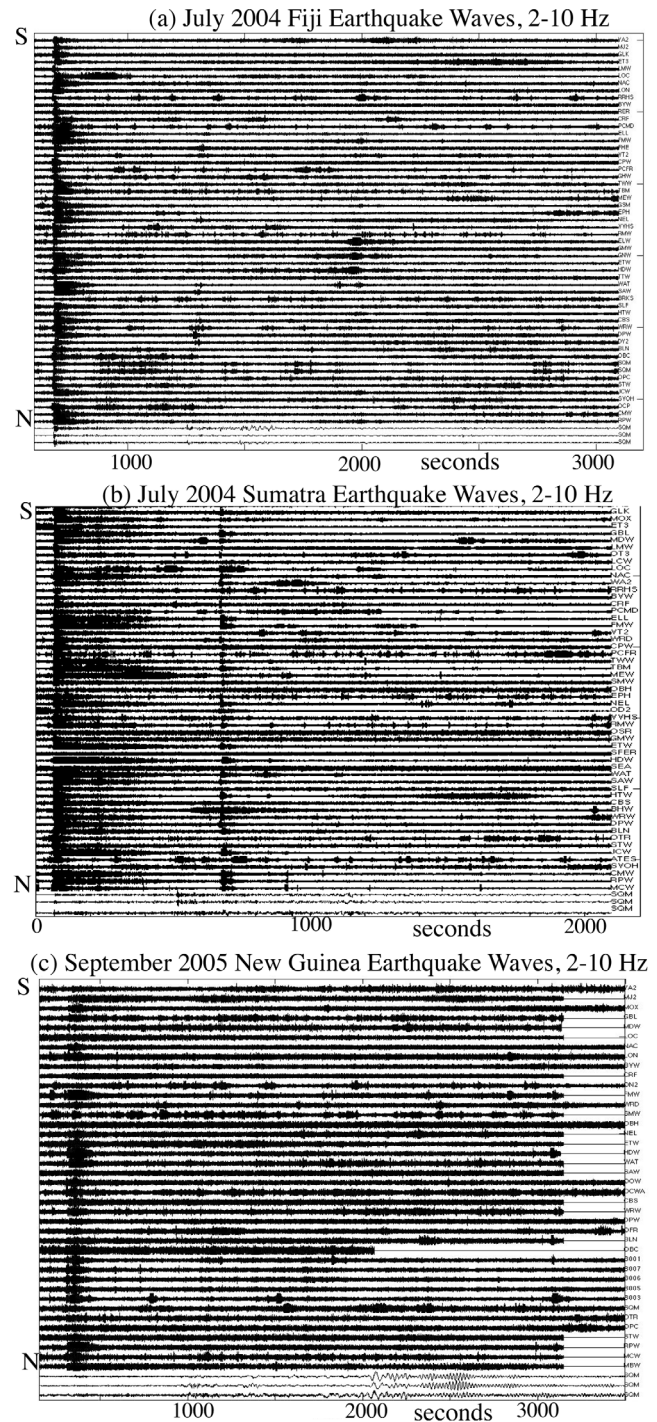


Figure 12. (a) Latitude-ordered record section of PNSN seismograms bandpass filtered between 2-10 Hz for the time interval in which waves from the 2004 Fiji earthquake (Table 1) traversed the region. 3-component broadband seismograms recorded at station SQM (bottom) show when posited triggering waves arrive. (b) Same plot as Figure 12a except for the 2004 Sumatra earthquake. (c) Same plot as Figure 12a except for the 2005 New Guinea earthquake. Coherent pulses, particularly evident in Figure 12b, and most P-wave energy vanish in the 5-13 Hz passband suggesting they all originate at the source rather than being triggered tremor.

Table 2. Summary of Triggered Tremor Observations^a

Source of Posited Triggering Waves	Tremor Triggered	Ambient Tremor Rate	Peak Velocity Relative to Reference*	Comments
<i>Northern Cascadia (Vancouver Island)</i>				
*M7.5 1999 Oaxaca, Mexico	Yes	Max	100%	
M7.6 2000 Volcano Island	Yes	Low	50%	
M7.9 2002 Denali, Alaska	Yes	Low	2500%	
M8.3 September 2003 Tokachi-Oki	No	Elevated	200%	Sporadic tremor observed ~4 hrs after waves arrive and lasts <1 day.
M9.1 2004 Sumatra	Yes	Low	300%	
M8.8 2010 Chile	Yes	Max	100%	
<i>Central Cascadia</i>				
M7.9 2002 Denali, Alaska	No	Low	1000%	
M7.1 2004 Fiji	No	Max	<25%	
M7.3 7/2004 Sumatra	No	Max	<25%	
M7.9 12/2004 Sumatra	Unclear	Low	400%	
M7.6 2005 New Guinea	No	Max	25%	
M8.1 2007 Kuril Islands	No	Elevated	200%	Preceded GPS-identified onset of 2007 ETS event by ~week. Tremor visible during wave train but does not correlate with any arrivals or modulated by the surface waves.
M7.5 2007 Molucca Sea	No	Max	10%	
M8.0 2007 Peru	No	Low	100%	
M6.6 2008 Alaska	No	Elevated	8%	
M6.7 2008 Guam	No	Max	5%	
*M7.9 2008 Wenchuan, China	Yes	Max	100%	

^aFor the waves radiated by each teleseism listed (left column) seismic data from the PNSN were examined for triggered tremor (see text). The results of this examination (second column from the left) and a qualitative description of the ambient tremor rate at the time wave from each earthquake passed are noted (middle column, with some comments in the right column). “Max” indicates waves arrived in the middle of an ETS event. The peak velocity of the teleseismic waves are noted relative to the one event in each data set that occurred during an ETS and triggered tremor, the Oaxaca and Wenchuan earthquakes for the northern and central Cascadia data sets, respectively.

from the M8.1 Kuril Islands earthquake arrived just prior to the 2007 ETS event, and failed to trigger tremor despite being twice as large as those from the triggering Wenchuan earthquake (Figure 7). I suggest that their failure to trigger reflected the lower, sputtering, ambient tremor rate and lack of detectable slow-slip when the Kuril Island earthquake waves arrived (Figure 5, Table 2). As Figures 7 and 8 illustrate, the 2007 M8.0 Peru earthquake also sent waves of comparable amplitude to those from the triggering Wenchuan earthquake (Figure 7), but during a time of no detectable tremor. Relative to the tremor rate and wave amplitudes associated with the triggering Wenchuan earthquake waves, the large Kuril Islands and comparable-sized Peru earthquake waves arrived during times of low to no ambient tremor rates, respectively. Their failure to trigger tremor provides corroboration of the clock-advance model.

[40] Many of the cases examined during ETS events are consistent with the size of the triggering wave being important as well as the amplitude. No triggered tremor can be seen during the three $M > 7$ teleseismic wave trains that arrived during 2004 and 2005 ETS events (Table 2), despite their arrival well after the onset of GPS-identified slow slip (Figure 6). Both the 2004 earthquakes were deep (Table 1) and thus generated fundamental-mode surface waves that are smaller than the body-wave arrivals (see Figure 12) and 10–15 times smaller than the peak amplitudes of the Wenchuan waves. The largest surface waves of these three events, from the shallowest 2005 New Guinea earthquake, are about four times smaller than those of the Wenchuan earthquake. Similarly, waves from the M7.5 Molucca Sea earthquake that occurred during the 2007 ETS event failed to trigger tremor. These had peak amplitudes an order of

magnitude smaller than the Wenchuan waves. Other than those from the Wenchuan earthquake, the largest waves to arrive during the 2008 ETS episode were from two $M \sim 6.6$ teleseisms, in Guam and Alaska. Although closer than the Wenchuan earthquake, their wave amplitudes at SQM were about 20 and 12 times smaller, respectively (Figure 13), and no triggered or ambient tremor is observed during the time

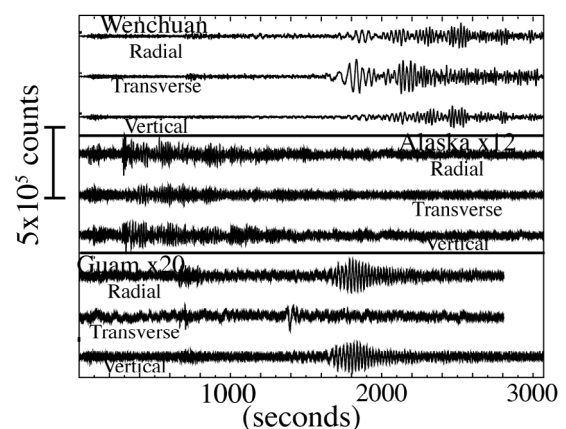


Figure 13. Broadband, 3-component waveforms of the 2 earthquakes that occurred at the onset (the Alaska earthquake) and during the 2008 ETS event (the Guam earthquake), and for reference, of the triggering 2008 Wenchuan earthquake (top). All data were recorded at station PNSN station SQM. A single amplitude scale is used, but the seismograms for the Alaska and Guam earthquakes have been scaled by the amounts listed.

periods when waves from these arrived (not shown). The tremor rate was sputtering when waves arrived from the Alaska earthquake and the Guam earthquake occurred when ambient tremor activity was vigorous (Figure 6). It may also be noteworthy that waves from the Guam and Alaska earthquakes differed from the Wenchuan waves in other aspects, with the Guam waveforms almost entirely composed of Rayleigh waves in contrast to the largest Wenchuan amplitudes being Love waves, and the dominant frequency of the Alaska waves is higher (Figure 13).

3.2. Testing the Clock-advance Model Using Tremor Amplitudes

[41] The clock-advance model also predicts that larger amplitude tremor should result from larger amplitude triggering deformations, assuming reasonably that larger waves are more effective triggers. A larger perturbation should cause more faults to fail sooner, and if there is little or no delay, the signals from these will superpose. I have examined this prediction for the five cases of triggered tremor. The result of a test of this hypothesis was only suggestive of consistency, largely because of scant noisy data.

[42] For each of the five triggering earthquakes, I plot the peak vertical velocities measured at each station that recorded tremor as a function of the maximum amplitude of the triggering broadband waves. I use data from station PHC for the tremor triggered in northern Cascadia and station SQM for the one case of triggered tremor in central Cascadia (Figure 14a). I attribute the tremendous scatter in the amplitudes for each triggering earthquake mostly to site effects (i.e., local focusing, amplification, or attenuation) and perhaps noise. I infer this because there is little correlation between amplitude and distance from the tremor source, expected as a result of attenuation and spreading. I apply site corrections derived by measuring the average noise amplitudes at each station from multiple time windows when no known signals should have arrived, each measured in the same manner as the tremor. I then assumed that the station with the lowest average noise level had the smallest site effects, and scaled all the other station measurements by the ratio of their average noise level to that at this quietest station (Figure 14b). This reduced the scatter for each earthquake by factors of 2 to 10, and although not perfect, the amplitudes now correlate with distance.

[43] These measures of tremor versus triggering wave amplitudes do not reveal a definitive trend, although the measurements for four of the five triggering earthquakes are suggestive of a positive correlation. Figure 14 also highlights the importance of assumptions about detection thresholds. That is, tremor signal amplitudes appear to be close to the minimum noise levels such that small increases in noise may result in tremor that is no longer detectable.

4. Discussion

4.1. Observations and Inferences From Parkfield, California

[44] Additional tests of the clock-advance model are provided by the recent study of triggered tremor in Parkfield, California by *Peng et al.* [2009]. They find a correlation between catalogued tremor rate increases and the occurrence of triggered tremor. This correlation supports a

clock-advance model, but only in a statistical sense. *Peng et al.* [2009] stack rates of catalogued tremor measured for 8 triggering and for 20 nontriggering earthquake wave trains, referenced to the arrival time of Love waves for each earthquake (see their Figure 15). They find a statistically significant rate increase at the Love wave arrival time only for the stacked rate derived for the 8 tremor-triggering earthquakes. They infer that the waves themselves perturbed the rates rather than the ambient rate being elevated prior to their arrival, but there is insufficient resolution to discriminate among these choices.

[45] Although statistically consistent with predictions of the clock-advance model, some of the individual catalogued tremor rate and triggered tremor observations of *Peng et al.* [2009] are inconsistent with the model. In Figure 15 I plot the fraction of a day in which tremor was observed along with the origin times of the 31 teleseisms studied by *Peng et al.* [2009]. The set includes all $M > 7.5$ earthquakes within 1,000 km of broadband station PKD within the time span of that study. I note several examples in which the clock-advance model predictions appear inconsistent with the observations in Figure 15 (others exist but aren't discussed). The triggering 2001 Kunlun waves are smaller than the approximate triggering threshold *Peng et al.* [2009] inferred, yet no ambient tremor is catalogued at this time. Waves arriving in 2007 failed to trigger, even though they were comparable or larger relative to those from the triggering 2006 Tonga and the ambient tremor rate was comparable or greater. In summary, the underlying process appears to be more complex than the simple clock-advance model implies, such that if correct, the complexities only average out when sufficient data are stacked.

4.2. Inferences About the Underlying Failure Mechanism

[46] The results documented herein suggest a failure mechanism for each source involving time-dependent nucleation, such as velocity and/or slip-dependent frictional models [*Beeler and Lockner, 2003*]. While simple Coulomb failure is consistent with many features of triggered and ambient tremor, it is inconsistent with tremor rate observations more strongly correlating with stress than stressing rate and with possible delayed failure. The Coulomb failure model predicts a correlation of failure, or seismicity, rate with stressing rate because the model assumes a constant failure stress threshold. Thus, as stressing rate increases, the failure threshold is reached more often, resulting in a higher seismicity rate.

[47] Coulomb failure occurring in sync with peak shear stresses from a passing seismic wave can occur on one specialized case, noted in *Hill* [2008]. If the stress drop of the triggered source is approximately the same size as the peak wave stress, subsequent cycles of the wave stresses will be sufficient to bring the source to failure repeatedly, resulting in a sequence of triggered events that are in phase with the peak dynamic shear stress. This requires appropriately oriented faults within a compressional environment, and repeated failure of the same source with extremely low stress drops (see Figure 15 of *Hill* [2008]). While these conditions may be satisfied for tremor in Cascadia, the variety of observations of triggering correlating with stres-

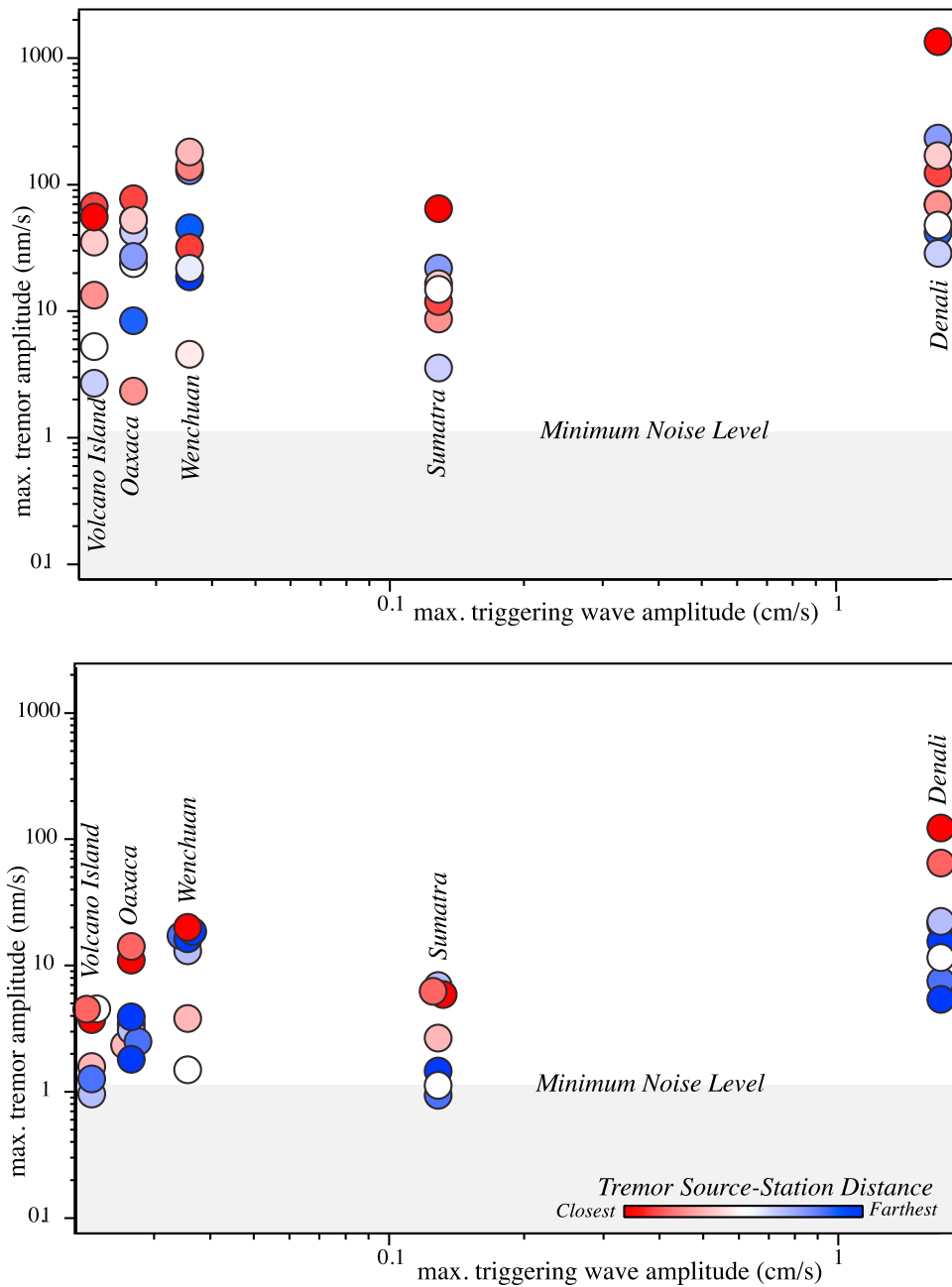


Figure 14. Triggered tremor amplitudes versus triggering wave amplitudes. Peak vertical velocity tremor amplitudes in the 5–13 Hz passband (left axes) measured at all stations that recorded tremor for each of the five triggering earthquakes in Cascadia versus the peak broadband velocity at PNSN station SQM for the Wenchuan earthquake and at CNSN station PHC for the other four events. The broadband measurements are from Euclidean amplitudes (square root of the sum of the squared three components) and tremor amplitudes are measured from envelopes processed as in Figure 3. The gray zone indicates the noise level at the quietest station, estimated from samples of noise only at all the stations processed in the same way as the tremor and averaged. Measured amplitudes were converted from counts to ground velocities using nominal instrumental sensitivities without removing that phase response. (a) Raw measurements, color-coded according to the distance from the tremor sources (color bar in Figure 6b). (b) Measurements in Figure 6a scaled by “site corrections” derived from noise samples (see text).

sing amplitudes rather than rates noted below argues against this specialized explanation.

[48] Mechanisms involving time-dependent nucleation predict an increased seismicity rate as loading amplitude

increases because in these models, the threshold for failure of each source often depends on the loading displacement and/or velocity (i.e., raising the loading rate increases the failure stress so the seismicity rate does not necessarily

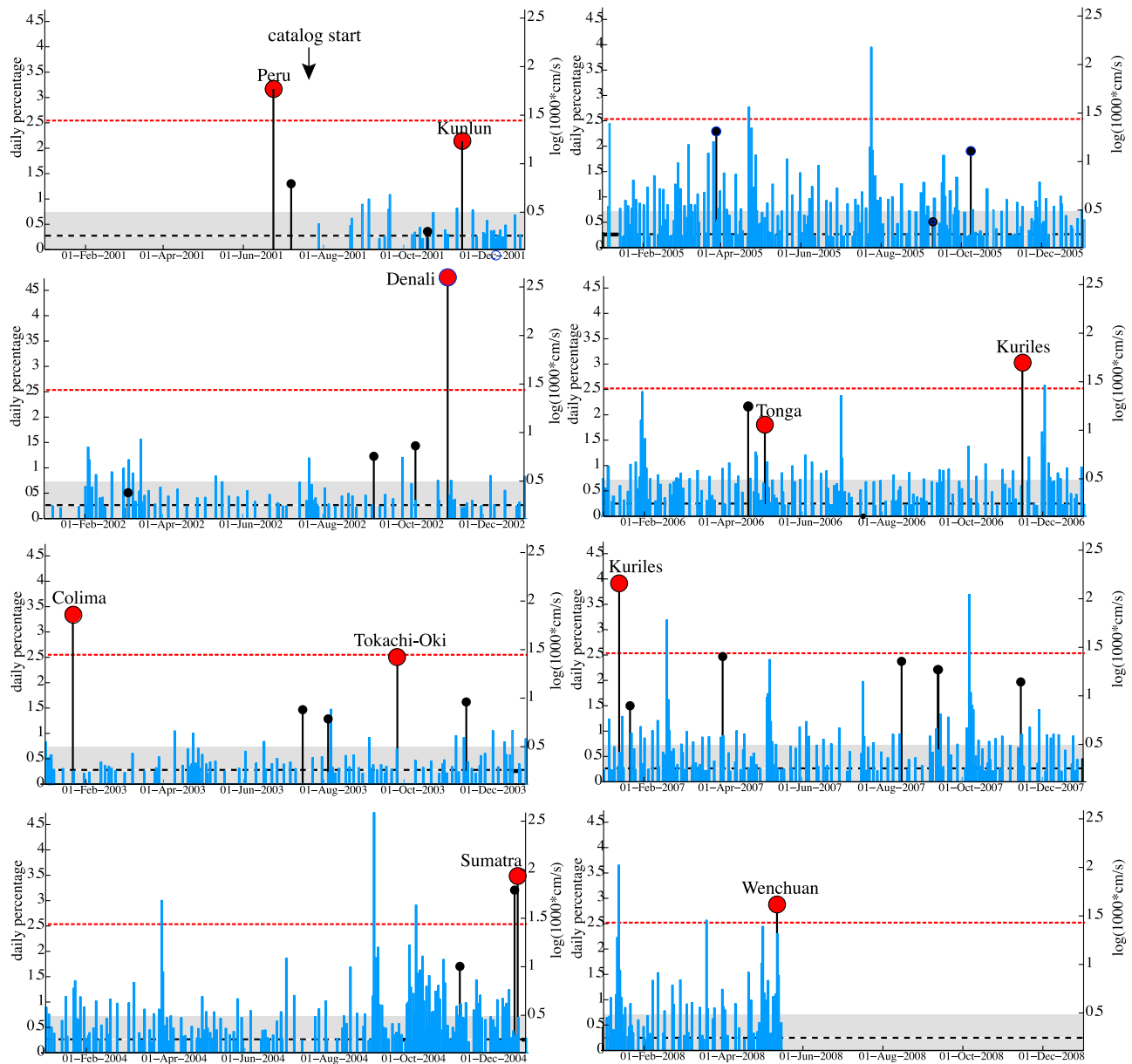


Figure 15. Vertical bars (blue) represent the fraction (in percent) of each day that have catalogued tremor from the Parkfield, California region. Each frame represents 1 year, with the mean daily percentage tremor was observed and +1 standard deviation shown by the horizontal black dashed line and grey band, respectively. At the ends of 2003 and 2004 yellow lines lasting a few days correspond to times of vigorous aftershocks when no tremor was catalogued. Stems with circles indicate the times of teleseismic earthquakes examined in *Peng et al.* [2009] study of triggered tremor, with small black and larger red circles indicating earthquakes that did not and did trigger tremor, respectively. The height of each symbol indicates the peak transverse velocity measured for the waves arriving at station PKD from each earthquake (right axes). The red dashed line marks the approximate triggering threshold inferred in *Peng et al.* [2009].

increase). Empirical studies of tidal triggering [*Cochran et al.*, 2004], laboratory experiments of stick-slip behavior under oscillatory loading [*Lockner and Beeler*, 1999; *Savage and Marone*, 2007, 2008], and numerical modeling invoking rate-state friction to explain these observations [*Beeler and Lockner*, 2003] all show that the seismicity rate correlates with the loading amplitude. My observations that the tremor rates correlate with stress rather than stressing rate are con-

sistent with other studies in Cascadia [*Rubinstein et al.*, 2007; *Lambert et al.*, 2009] and elsewhere [*Peng et al.*, 2008; *Miyazawa et al.*, 2008; *Thomas et al.*, 2009]. In these studies wave- or tide-associated stresses can be inferred at the tremor source and triggered tremor bursts occur at the peak shear and/or normal stresses, not at peak stressing rates. One exception to this is the study of *Nakata et al.* [2008], in which tremor rates in the Shikoku region of

Japan were found to have the same periodicity as the tides but were not in phase with either the tidal stresses (any component) or stressing rates. The gradual increase of measured ambient tremor rate during ETS events (Figures 5 and 6) also suggests a correlation with stress rather than stressing rate. This assumes ambient tremor is driven by slow slip and stress, which also appear to increase gradually as inferred from geodetic data.

5. Conclusions

[49] The results of this and previous studies provide constraints on the failure mechanisms likely involved in generating tremor. They demonstrate that the conditions suitable for tremor generation exist in a wide range of tectonic environments, but also only in very localized volumes. These conditions must involve properties that change temporally because different tremor sources are triggered by earthquake wave trains that appear to be similar but occur at different times. The occurrence of failure within seconds after the application of a failure-favoring triggering wave (e.g., in the direction of tectonic loading if shear failure) implies that if fluids are involved, the distances they can travel are likely considerably less than a meter. The degree to which delayed failure and secondary triggering (by tremor waves) occurs is highly uncertain, but is likely not significant. Both shear and dilatational deformations appear able to trigger tremor. Triggered and ambient tremor correlate more strongly with stress than stressing rate, suggesting tremor results from time-dependent weakening processes (e.g., frictional failure), rather than simple Coulomb failure.

[50] I envision a model in which tremor radiates from a population of sources or fault patches of relatively small, uniform size (Figure 4). In this model the patches are driven to failure directly or indirectly by plate motions and slow slip on a major fault, and radiate “ambient” tremor. The tremor patches may lie on the slowly slipping fault or may be distributed in its vicinity. A passing seismic wave also may bring a patch, or patches, to failure, manifesting as triggered tremor. In essence, triggered tremor events are simply ambient ones that failed early, or clock-advanced failure events. The clock-advance model predicts that the probability of triggering tremor is proportional to the product of the ambient tremor rate and a function describing the efficacy of the triggering wave to initiate a tremor event. I have tested this model prediction primarily by comparing of a suite of teleseismic waves that did and did not trigger tremor with measured ambient tremor rates, and assumed that the efficacy of each wave train should scale with its peak amplitude. I summarize below the consistency of the evidence with predictions of the clock-advance model, noting the inconsistencies explicitly.

[51] When the ambient rate was maximal, during ETS events, of the five large teleseismic wave trains in the central Cascadia data set (from the 2004 Fiji, 2005 New Guinea, 2007 Molucca Sea, 2008 Guam, and 2008 Wenchuan earthquakes) only the Wenchuan earthquake triggered tremor. However, the amplitudes of the other four large amplitude teleseismic wave trains that arrived during ETS events were four times to more than an order of magnitude smaller than those from the Wenchuan earthquake. I conclude that even when there is an abundance of read-to-fail-

sources, wave amplitudes must exceed $\sim 25\%$ that of the Wenchuan earthquake to trigger detectable tremor (see Table 2). In the northern Cascadia data set, at the time this study was completed, only the wave train from the 1999 Oaxaca earthquake passed through during an ETS event and it triggered tremor. The tremor sources triggered by the Wenchuan and Oaxaca earthquake waves were located within the corresponding distribution of ambient tremor sources. Waves from these two events serve as references for each data set. Fortunately, while revising this paper the 27 Feb 2010 M8.8 Chilean earthquake sent waves of roughly the same peak amplitude as those from the 1999 Oaxaca earthquake (vertical component peak velocities from both earthquakes were ~ 0.4 mm/s at station PHC) through a small area of Vancouver Island that was experiencing vigorous tremor activity. Although smaller than one of the expected ETS episodes that occurs ~ 14 months in this part of Cascadia, geodetic deformation of several mm was noted several days later. Triggered tremor modulated by the Chilean earthquake surface waves was clear at the CNSN stations surrounding the ambient tremor, in accord with the predictions of the clock-advance model.

[52] All waves that arrived when the ambient rate was elevated, but anemic relative to the rate in the midst of an ETS event, failed to trigger tremor. Among the wave trains in this class, one wave train in the central Cascadia data set (from the July 2004 Sumatra earthquake) had smaller amplitudes than those of the reference 2008 Wenchuan earthquake waves. The nearly doubled amplitudes of two wave trains relative to reference triggering waves (from the 2007 Kuril Island and the 2003 Tokachi-Oki earthquake waves in the central and northern Cascadia data sets, respectively) appear to not have been sufficient to compensate for the smaller ambient rate.

[53] When little or no ambient tremor was detected, in the northern Cascadia data set waves from seven earthquakes had the same or greater amplitudes than those from the triggering waves of the Oaxaca earthquake. Only those with the two largest peak amplitudes triggered tremor (from the 2002 Denali and December 2004 Sumatra earthquakes). *Rubinstein et al.* [2009] suggested their extraordinarily large amplitudes effectively compensated for the low ambient rate. The peak amplitudes of the Sumatra waves were $\sim 300\%$ bigger than those of triggering reference wave. In the central Cascadia data set, only one example of waves that arrived when no ambient tremor was catalogued was examined carefully (the 2007 Peru earthquake), and although its peak amplitude was comparable to the triggering reference Wenchuan waves, it failed to trigger tremor. One wave train with smaller peak amplitudes than those from the Oaxaca earthquake, from the 2000 Volcano Island earthquake, triggered tremor and is clearly inconsistent with the predictions of the clock-advance model.

[54] I also attempted to test the clock-advance model prediction that larger triggering waves should result in larger triggered tremor signals. This assumes that more tremor sources will fail, radiate, and superpose for larger loads. The results for the five cases of triggered tremor in Cascadia do not conform to this prediction, noting however, that the measurements themselves have significant uncertainties. This is largely due to the low signal-to-noise ratios of the tremor signals and likely site effects in

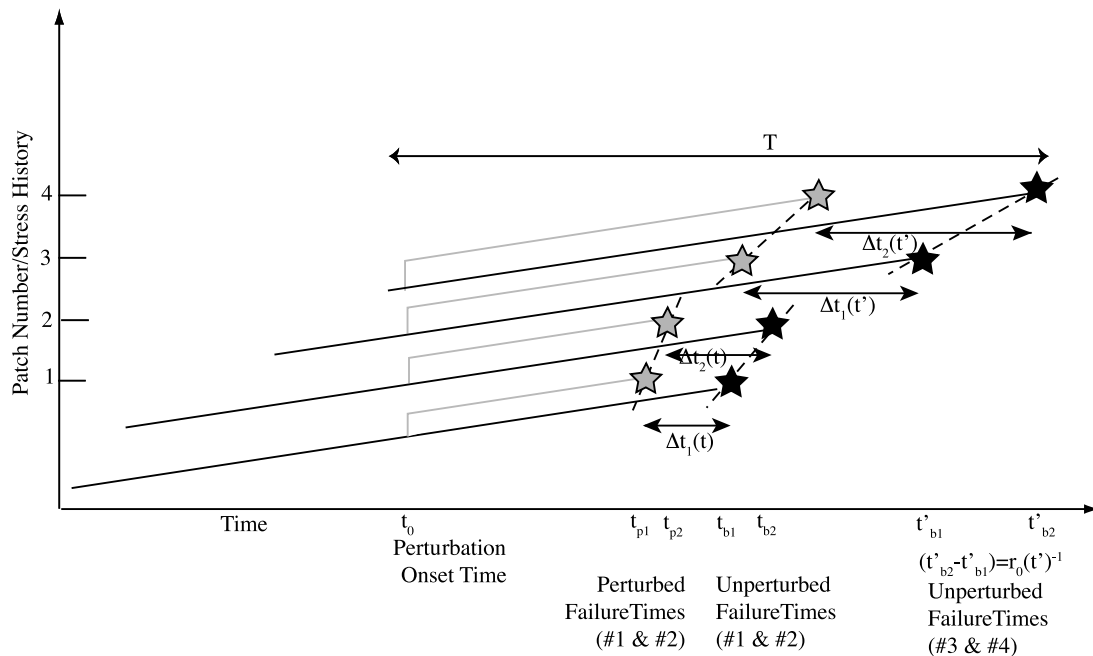


Figure A1. Schematic of the loading and failure process for four patches (faults) loaded at constant rate (black lines) and subjected to a step increase in stress (grey lines) at time t_0 . Stars represent failure times for each patch. See text for explanation.

the tremor frequency band. Other observational limitations that could be reduced with future studies include catalog heterogeneity and sensitivity of triggered tremor identification to detection threshold.

[55] Many of the observations from Cascadia are qualitatively consistent with the clock-advance model, but one clearly violates it. Definitive inferences about the relative dependences of the triggering probability on ambient rate and on wave amplitude (and other wave characteristics) will require additional, more quantitative measures of both than are presently possible. Undoubtedly too, the tremor source process is a more complex system than that which the clock-advance model describes.

Appendix A

[56] Figure A1 illustrates schematically how the instantaneous failure, or seismicity, rate relates to a clock-advance model. For simplicity, I illustrate this for a population of just four patches (faults) loaded at a constant rate and subjected to a step stress increase at time t_0 . All the patches have identical unperturbed recurrence (cycle) times, T . The same schematic and notation is used in *Gomberg et al.* [2000] but here I use four patches instead of two to show that the background (ambient) rate may be temporally varying. The length of each diagonal line represents the loading history of each patch, shown for a single failure cycle for each patch (perturbed paths shown in grey lines).

[57] The instantaneous failure rate is simply the inverse of the inter-event time between temporally adjacent patches failing (noted by the subscripted numbers); i.e., in Figure A1 the slopes of the dashed lines between successive failures

are the instantaneous rates. Mathematically, the unperturbed and perturbed rates are

$$r_0 = \Delta^n / (t_{b(i+\Delta n)} - t_{bi}) \quad \text{and} \quad r = \Delta^n / (t_{p(i+\Delta n)} - t_{pi}) \quad (\text{A1})$$

respectively, with unperturbed and perturbed failure times for each patch t_b and t_p , respectively, and Δn is the number of patches that fail between times $t_{b(i+\Delta n)}$ and t_{bi} . For an instantaneous rate, $\Delta n=1$.

[58] The changes in rates, r/r_0 , due to a perturbation arise because the clock-advances, Δt , depend on where each patch is in its cycle when perturbed (i.e., the time between t_0 and the start of the cycle), which differs for each patch. The perturbed rate varies temporally both because Δt is not constant and because the unperturbed rate also is temporally varying. Following *Gomberg et al.* [2000, 2005], for each patch $t_p = t_b - \Delta t$, so that the perturbed instantaneous rate is

$$\begin{aligned} r^{-1} &= (t_{p(i+1)} - t_{pi}) = [(t_{b(i+1)} - \Delta t_{(i+1)}) - (t_{bi} - \Delta t_i)] \\ &= [(t_{b(i+1)} - t_{bi}) - (\Delta t_{(i+1)} - \Delta t_i)] \\ &= r_0^{-1} - (\Delta t_{(i+1)} - \Delta t_i) = r_0^{-1} [1 - \Delta \Delta t / \Delta t_b] \end{aligned} \quad (\text{A2})$$

This leads to equation (1) describing the instantaneous rate, noting that the change in the unperturbed failure time for $\Delta n=1$ is the same as the change in cycle time T , and writing equation (A2) in differential form:

$$\begin{aligned} r(t) &= r_0(t - \Delta t) [1 - \Delta \Delta t / \Delta t_b]^{-1} \\ &= r_0(t - \Delta t) [1 - d\Delta t(t) / dt_b]^{-1} = r_0 [1 - d\Delta t(t) / dT]^{-1} \end{aligned} \quad (\text{A3})$$

t is the time passed from the application of the perturbation.

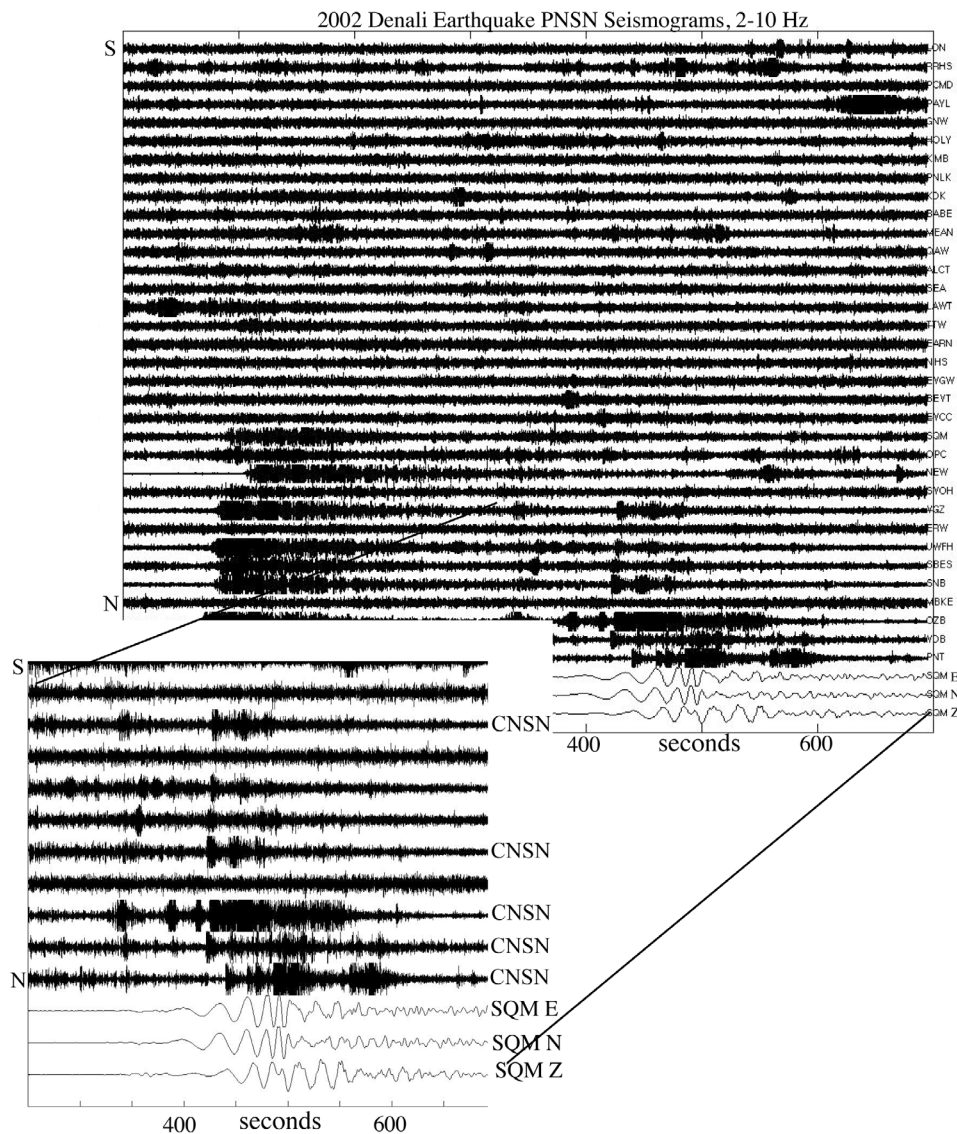


Figure B1. Latitude-ordered record section of PNSN seismograms bandpass filtered between 2–10 Hz for the time interval in which waves from the 2002 Denali earthquake (Table 1) traversed the region. Three-component broadband seismograms recorded at station SQM (bottom) show when posited triggering waves arrive. The expanded plot shows that data contributed from CNSN stations (labeled) record the tremor (and earthquakes) signals with greater fidelity; signals can only be seen in data from two PNSN stations despite being at the same or farther distance from the sources.

[59] The requirements for the clock-advance model to produce a finite-duration rate change include a distribution of clock advances in which sources that are farther from failure when perturbed experience greater clock advances. Finite duration in this context implies that $r/r_0 > 1$ for a time period that exceeds the duration of the perturbation, such as in an aftershock sequence that may last for days to years after the causative main shock. This specific dependence of Δt on the proximity to failure is only predicted for particular failure models and perturbations. For reasons noted below, any model involving self-accelerating failure, such as rate-state friction or critical crack growth, only predicts this dependence for static (step-function) stress perturbations and not for transient perturbations [Gomberg, 2001]. A

Coulomb failure model does not predict this dependence for any type of perturbation.

[60] The reason a distribution of values of Δt is required becomes clear by noting that if all patches are clock-advanced identically the perturbed inter-event times and the failure rate do not change. This is true for a Coulomb model, except for patches that were within Δt from failure at the time the perturbation was applied and that fail immediately, resulting an instantaneous spike in failure rate. This requirement can also be understood in terms of equation (A2), noting that the term $(\Delta t_{i+1} - \Delta t_i) = 0$ so that $r/r_0 = 1$. Graphically, in Figure A1, if Δt is the same for all patches (i.e., the double-headed arrows all are the same length), the slope describing

the instantaneous failure rate does not change when perturbed.

[61] The requirement that sources that are farther from failure when perturbed experience greater clock advances so that $r/r_0 > 1$ can be understood in terms of equations (A2) and (A3), noting that $r/r_0 > 1$ requires that the difference or differential terms in Δt must be positive. The dependence of Δt on the proximity to failure drawn in Figure A1 satisfies this requirement; that is, the $(i+1)$ th patch is farther from failure than the i th patch at t_0 and $\Delta t_{i+1} > \Delta t_i$. One can see graphically that if instead $\Delta t_{i+1} < \Delta t_i$, the slope representing the instantaneous rate would become less steep rather than steeper, implying $r/r_0 < 1$. Physically, for self-accelerating failure models, more mature (closer to failure) sources are more sensitive to perturbations. Despite this, for the static perturbation shown in Figure A1, the effects of the perturbation accrue for longer on patches that have longer to wait until reaching failure levels, and thus they experience greater clock advances. For transient perturbations, the accrual time is the duration of the transient and thus is the same for all sources (unless they fail during the transient), so that the more mature faults at t_0 have larger clock advances, or $\Delta t_{i+1} < \Delta t_i$ and $r/r_0 < 1$. See *Gomberg* [2001] for a more detailed discussion.

Appendix B: Detection in Central Cascadia

[62] Although no tremor catalog exists for the time periods spanning the 2002 M7.9 Denali, Alaska and 2004 M9.1 Sumatra earthquakes, I examine PNSN waveform data for these because, like on Vancouver Island, the amplitudes of waves from these two earthquakes were probably the largest among all teleseismic disturbances to traverse the central Cascadia region in decades. Smaller, more local earthquakes undoubtedly generated larger wave amplitudes in their epicentral vicinity, but not over the entire network. In addition, these examples highlight the challenges of identifying tremor and of making comparisons between regions monitored by different networks. Waves from both earthquakes triggered clear tremor originating from a source at the north end of Vancouver Island during times when ambient tremor was not detectable [*Rubenstein et al.*, 2009]. One thus wonders why no triggered tremor was observed in central Cascadia, within the boundaries of the PNSN?

[63] I suggest that the tremor detection threshold prior to 2005 was lower for Vancouver Island than western Washington, and that perhaps Denali-triggered and Sumatra-triggered tremor may have occurred in western Washington but went undetected. The PNSN network receives a few signals from the CNSN stations near the U.S.-Canadian border. The record section of Figure B1 shows that the tremor originating on Vancouver Island and Denali P-wave energy are clearest in the data from the CNSN stations at comparable distances and azimuths to the PNSN stations. The same result applies to the Sumatra data (not shown). In addition to apparently having a higher detection threshold, for the Denali earthquake in particular many of the PNSN stations clipped or appeared to be overdriven (even if on-scale when filtered above 2 Hz spikes appeared where the largest amplitudes occurred). The strong motion stations provided on-scale data, but filtering above 2 Hz seemed to remove the signal, possibly reflecting their more limited

dynamic range (i.e., they recorded only the larger, lower frequency energy with fidelity). A comparison of the tremor amplitudes triggered by the Denali earthquake on Vancouver Island and by the Wenchuan earthquake in the PNSN shows that in 2008 tremor signals an order of magnitude smaller than those triggered by Denali on Vancouver Island were detectable by the PNSN, but this undoubtedly was not the case in 2002 because the PNSN has changed significantly since then. A detailed study of the tremor detection thresholds is needed to be able to compare the triggering potential between regions. However, such a study but is beyond the scope of this one.

[64] **Acknowledgments.** The author would like to acknowledge the insightful reviews of Tom Parsons, David Hill, Zhiqiang Peng, Nick Beeler, Paul Johnson, and several anonymous reviewers. Catalogs were provided by Honn Kao of the Geological Survey of Canada, Aaron Wech of the University of Washington, and Robert Nadeau of the University of California at Berkeley. Seismic waveform data were provided by the Canadian National Seismic Network, Geological Survey of Canada, the Pacific Northwest Seismic Network, University of Washington, and the Incorporated Research Institutions for Seismology (IRIS).

References

- Aguiar, A. C., T. I. Melbourne, and C. Scrivner (2009), Moment rate during Cascadia tremor constrained by GPS, *J. Geophys. Res.*, *114*, B00A05, doi:10.1029/2008JB005909.
- Audet, P., M. G. Bostock, N. I. Christensen, and S. M. Peacock (2009), Seismic evidence for overpressured subducted crust and megathrust fault sealing, *Nature*, *457*, 76–78, doi:10.1038/nature07650.
- Beeler, N. M., and D. A. Lockner (2003), Why earthquakes correlate weakly with the solid Earth tides: Effects of periodic stress on the rate and probability of earthquake occurrence, *J. Geophys. Res.*, *108*(B8), 2391, doi:10.1029/2001JB001518.
- Beeler, N. M., T. E. Tullis, A. K. Kronenberg, and L. A. Reinen (2007), The instantaneous rate dependence in low temperature laboratory rock friction and rock deformation experiments, *J. Geophys. Res.*, *112*, B07310, doi:10.1029/2005JB003772.
- Belardinelli, M. E., A. Bizzarri, and M. Cocco (2003), Earthquake triggering by static and dynamic stress changes, *J. Geophys. Res.*, *108*(B3), 2135, doi:10.1029/2002JB001779.
- Cochran, E. S., J. E. Vidale, and T. Sachiko (2004), Earth tides can trigger shallow thrust fault earthquakes, *Science*, *306*, 1164–1166.
- Dieterich, J. (1994), A constitutive law for rate of earthquake production and its application to earthquake clustering, *J. Geophys. Res.*, *99*(B2), 2601–2618, doi:10.1029/93JB02581.
- Felzer, K. R., R. E. Abercrombie, and G. Ekström (2003), Secondary aftershocks and their importance for aftershock prediction, *Bull. Seismol. Soc. Am.*, *93*, 1433–1448.
- Felzer, K. R., and E. E. Brodsky (2006), Decay of aftershock density with distance indicates triggering by dynamic stress, *Nature*, *441*, 735–738, doi:10.1038/nature04799.
- Gomberg, J. (2001), The failure of earthquake failure models, *J. Geophys. Res.*, *106*, 16,253–16,264, doi:10.1029/2000JB000003.
- Gomberg, J., J. L. Rubinstein, Z. Peng, K. C. Creager, J. E. Vidale, and P. Bodin (2008), Widespread triggering of non-volcanic tremor in California, *Science*, *319*, 173.
- Gomberg, J., N. M. Beeler, M. L. Blanpied, and P. Bodin (1998), Earthquake triggering by transient and static deformations, *J. Geophys. Res.*, *103*(B10), 24,411–24,426, doi:10.1029/98JB01125.
- Gomberg, J., N. M. Beeler, and M. L. Blanpied (2000), On rate-and-state and Coulomb failure models, *J. Geophys. Res.*, *105*(B4), 7857–7872, doi:10.1029/1999JB900438.
- Gomberg, J., P. Reasenberg, M. Cocco, and M. E. Belardinelli (2005), A frictional population model of seismicity rate change, *J. Geophys. Res.*, *110*, B05S03, doi:10.1029/2004JB003404.
- Hardebeck, J. L. (2004), Stress triggering and earthquake probability estimates, *J. Geophys. Res.*, *109*, B04310, doi:10.1029/2003JB002437.
- Helmstetter, A., Y. Y. Kagan, and D. D. Jackson (2005), Importance of small earthquakes for stress transfers and earthquake triggering, *J. Geophys. Res.*, *110*, B05S08, doi:10.1029/2004JB003286.
- Ide, S., G. C. Beroza, D. R. Shelly, and T. Uchide (2007), A scaling law for slow earthquakes, *Nature*, *447*, 76–79.
- Ide, S., K. Imanishi, Y. Yoshida, G. C. Beroza, and D. R. Shelly (2008), Bridging the gap between seismically and geodetically detected

- slow earthquakes, *Geophys. Res. Lett.*, *35*, L10305, doi:10.1029/2008GL034014.
- Kaneko, Y., and N. Lapusta (2008), Variability of earthquake nucleation in continuum models of rate-and-state faults and implications for aftershock rates, *J. Geophys. Res.*, *113*, B12312, doi:10.1029/2007JB005154.
- Kao, H., and S. Shan (2004), The source-scanning algorithm: mapping the distribution of seismic sources in time and space, *Geophys. J. Int.*, *157*, 589–594.
- Lambert, A., H. Kao, G. Rogers, and N. Courtier (2009), Correlation of tremor activity with tidal stress in the northern Cascadia subduction zone, *J. Geophys. Res.*, *114*, B00A08, doi:10.1029/2008JB006038.
- La Rocca, M., K. C. Creager, D. Galluzzo, S. Malone, J. E. Vidale, J. R. Sweet, and A. G. Wech (2009), Cascadia tremor located near plate interface constrained by S minus P wave times, *Science*, *323*, 620–623.
- Lockner, D. A., and N. M. Beeler (1999), Premonitory slip and tidal triggering of earthquakes, *J. Geophys. Res.*, *104*(B9), 20,133–20,151, doi:10.1029/1999JB900205.
- Maeda, T., and K. Obara (2009), Spatio-temporal distribution of seismic energy radiation from low-frequency tremor in western Shikoku, Japan, *J. Geophys. Res.*, *114*, B00A09, doi:10.1029/2008JB006043.
- Marsan, D., and S. S. Nalbant (2005), Methods for measuring seismicity rate changes: A review and a study of how the Mw 7.3 Landers earthquake affected the aftershock sequence of the Mw 6.1 Joshua Tree earthquake, *Pure Appl. Geophys.*, *162*, 1151–1184, doi:10.1007/s00024-004-2665-4.
- Marsan, D., and O. Lengline (2008), Extending earthquakes' reach through Cascading, *Science*, *319*, 1076–1079.
- McCausland, W. A., E. Roeloffs, and P. Silver (2008), New insights into Cascadia slow slip events using Plate Boundary Observatory borehole strainmeters, Fall Meet. Suppl., Abstract G21B-0691, *Eos Trans. AGU*, *89*(53),
- Miyazawa, M., and E. E. Brodsky (2008), Deep low-frequency tremor that correlates with passing surface waves, *J. Geophys. Res.*, *113*, B01307, doi:10.1029/2006JB004890.
- Miyazawa, M., E. E. Brodsky, and J. Mori (2008), Learning from dynamic triggering of low-frequency tremor in subduction zones, *Earth Planets Space*, *60*, e17–e20.
- Miyazawa, M., and J. Mori (2005), Detection of triggered deep low-frequency events from the 2003 Tokachi-ochi earthquake, *Geophys. Res. Lett.*, *32*, L10307, doi:10.1029/2005GL022539.
- Miyazawa, M., and J. Mori (2006), Evidence suggesting fluid flow beneath Japan due to periodic seismic triggering from the 2004 Sumatra-Andaman earthquake, *Geophys. Res. Lett.*, *33*, L05303, doi:10.1029/2005GL025087.
- Nakata, R., N. Suda, and H. Tsuruoka (2008), Non-volcanic tremor resulting from the combined effect of Earth tides and slow slip events, *Nature Geoscience*, *1*, 676–678, doi:10.1038/ngeo288.
- Obara (2009), Inhomogeneous distribution of deep slow earthquake activity along the strike of the subducting Philippine Sea Plate, *Gondwana Res.*, *16*, 512–526.
- Obara, K., H. Hirose, F. Yamamizu, and K. Kasahara (2004), Episodic slow slip events accompanied by non-volcanic tremors in southwest Japan subduction zone, *Geophys. Res. Lett.*, *31*, L23602, doi:10.1029/2004GL020848.
- Payero, J. S., V. Kostoglodov, N. Shapiro, T. Mikumo, A. Iglesia, X. Perez-Campos, and R. W. Clayton (2008), Nonvolcanic tremor observed in the Mexican subduction zone, *Geophys. Res. Lett.*, *35*, L07305, doi:10.1029/2007GL032877.
- Peng, Z., and K. Chao (2008), Non-volcanic tremor beneath the Central Range in Taiwan triggered by the 2001 Mw7.8 Kunlun earthquake, *Geophys. J. Int.*, *175*(2), 825–829, doi:10.1111/j.1365-246X.2008.03886.x.
- Peng, Z., J. E. Vidale, K. C. Creager, J. L. Rubinstein, J. Gomberg, and P. Bodin (2008), Strong tremor near Parkfield, CA excited by the 2002 Denali Fault earthquake, *Geophys. Res. Lett.*, *35*, L23305, doi:10.1029/2008GL036080.
- Peng, Z., J. E. Vidale, A. G. Wech, R. M. Nadeau, and K. C. Creager (2009), Remote triggering of tremor along the San Andreas fault in central California, *J. Geophys. Res.*, *114*, B00A06, doi:10.1029/2008JB006049.
- Peterson, C., D. Christensen, and S. McNutt (2007), Non-volcanic tremor in South-Central Alaska and its relation to the 1998–2000 slow-slip event, Fall Meet. Suppl., Abstract T11F-08, *Eos Trans. AGU*, *88*(52).
- Richardson, E., and C. Marone (2008), What triggers tremor?, *Science*, *319*, 166–167, doi:10.1126/science.1152877.
- Rogers, G., and H. Dragert (2003), Episodic tremor and slip on the Cascadia subduction zone: The chatter of silent slip, *Science*, *300*, 1942–1943.
- Rubinstein, J. L., J. E. Vidale, J. Gomberg, P. Bodin, K. C. Creager, and S. Malone (2007), Non-volcanic tremor driven by large transient shear stresses, *Nature*, *448*, 579–582, doi:10.1038/nature06017.
- Rubinstein, J. L., J. Gomberg, J. E. Vidale, A. G. Wech, H. Kao, K. C. Creager, and G. Rogers (2009), Seismic wave triggering of nonvolcanic tremor, episodic tremor and slip, and earthquakes on Vancouver Island, *J. Geophys. Res.*, *114*, B00A01, doi:10.1029/2008JB005875.
- Rubinstein, J. L., D. R. Shelly, and W. L. Ellsworth (2010), Non-volcanic tremor: A window into the roots of fault zones, in *New Frontiers in Integrated Solid Earth Sciences, International Year of Planet Earth*, edited by S. Cloetingh and J. Negendank, pp. 287–314, Springer Science+Business Media B.V, New York.
- Savage, H. M., and C. Marone (2007), Effects of shear velocity oscillations on stick-slip behavior in laboratory experiments, *J. Geophys. Res.*, *112*, B02301, doi:10.1029/2005JB004238.
- Savage, H. M., and C. Marone (2008), Potential for earthquake triggering from transient deformations, *J. Geophys. Res.*, *113*, B05302, doi:10.1029/2007JB005277.
- Segall, P., and J. R. Rice (2006), Does shear heating of pore fluid contribute to earthquake nucleation?, *J. Geophys. Res.*, *111*, B09316, doi:10.1029/2005JB004129.
- Thomas, A. M., R. M. Nadeau, and R. Burgmann (2009), Tremor-tide correlations and near-lithostatic pore pressure on the deep San Andreas fault, *Nature*, *462*, 1048–1051, doi:10.1038/nature08654.
- Voisin, C. (2002), Dynamic triggering of earthquakes: The nonlinear slip-dependent friction case, *J. Geophys. Res.*, *107*(B12), 2356, doi:10.1029/2001JB001121.
- Voisin, C., F. Cotton, and S. Di Carli (2004), A unified model for dynamic and static stress triggering of aftershocks, antishocks, remote seismicity, creep events, and multisegmented rupture, *J. Geophys. Res.*, *109*, B06304, doi:10.1029/2003JB002886.
- Voisin, C., J.-R. Grasso, E. Larose, and F. Renard (2008), Evolution of seismic signals and slip patterns along subduction zones: Insights from a friction lab scale experiment, *Geophys. Res. Lett.*, *35*, L08302, doi:10.1029/2008GL033356.
- Wech, A. G., and K. C. Creager (2008), Automated detection and location of Cascadia tremor, *Geophys. Res. Lett.*, *35*, L20302, doi:10.1029/2008GL035458.
- Wech, A. G., K. C. Creager, and T. I. Melbourne (2009), Seismic and geodetic constraints on Cascadia slow slip, *J. Geophys. Res.*, *114*, B10316, doi:10.1029/2008JB006090.

J. Gomberg, U.S. Geological Survey, Department of Earth and Space Sciences, University of Washington, Seattle, Washington 98195, USA. (gomberg@usgs.gov)